Received: 15 April 2021 | Revised: 20 July 2021 | Accepted: 15 August 2021

DOI: 10.1002/jev2.12140

RESEARCH ARTICLE

Formation of a protein corona on the surface of extracellular vesicles in blood plasma

Eszter Á. Tóth[1] | **Lilla Turiák**[2,3] | **Tamás Visnovitz**[1] | **Csaba Cserép**[4] | **Anett Mázló**[5] | **Barbara W. Sódar**[1,6] | **András I. Försönits**[1] | **Gábor Petővári**[7] | **Anna Sebestyén**[7] | **Zsolt Komlósi**[1] | **László Drahos**[2,3] | **Ágnes Kittel**[8] | **György Nagy**[1,9] | **Attila Bácsi**[5] | **Ádám Dénes**[4] | **Yong Song Gho**[10] | **Katalin É. Szabó-Taylor**[1] | **Edit I. Buzás**[1,2,6]

[1] Department of Genetics, Cell- and Immunobiology, Semmelweis University, Budapest, Hungary

[2] ELKH-SE Immune-Proteogenomics Extracellular Vesicle Research Group, Budapest, Hungary

[3] MS Proteomics Research Group, Research Centre for Natural Sciences, Eötvös Loránd Research Network, Budapest, Hungary

[4] Laboratory of Neuroimmunology, Institute of Experimental MedicineEötvös Loránd Research Network, Budapest, Hungary

[5] Department of Immunology, Faculty of Medicine, University of Debrecen, Debrecen, Hungary

[6] HCEMM-SE Extracellular Vesicles Research Group, Budapest, Hungary

[7] Tumour Biology, Tumour Metabolism Research Group, 1st Department of Pathology and Experimental Cancer Research, Semmelweis University, Budapest, Hungary

[8] Institute of Experimental MedicineEötvös Loránd Research Network, Budapest, Hungary

[9] Department of Rheumatology & Clinical Immunology, Semmelweis University, Budapest, Hungary

[10] Department of Life Sciences, Pohang University of Science and Technology (POSTECH), Pohang, Republic of Korea

Correspondence
Edit I. Buzás, Semmelweis University, Dept. of Genetics, Cell- and Immunobiology, 1085, Budapest, Üllői út 26, Hungary.
Email: buzas.edit@med.semmelweis-univ.hu

Katalin É Szabó-Taylor and Edit I Buzás contributed equally.

Funding information
National Research, Development and Innovation Office NKFIH, Hungary, Grant/Award Numbers: OTKA11958, OTKA120237, OTKA125337, OTKA K 131479, OTKA PD 121187, OTKA FK 131603, OTKA 131762, NVKP_16-1-2016-0017; Higher Education Institutional Excellence Program – Therapeutic development, Grant/Award Numbers: ÚNKP-19-3-I-SE-45, ÚNKP-20-5; New National Excellence Program of the Ministry for Innovation and Technology; Ministry for National Economy of Hungary, Grant/Award Numbers: VEKOP-2.3.2-16-2016-00002, VEKOP-2.3.3-15-2016-00016, EFOP-3.6.3-VEKOP-16-2017-00009; Az orvos-, egészségtudományi- és gyógyszerészképzés tudományos műhelyeinek fejlesztése; European Commission, Grant/Award Number: H2020-

Abstract

In this study we tested whether a protein corona is formed around extracellular vesicles (EVs) in blood plasma. We isolated medium-sized nascent EVs of THP1 cells as well as of Optiprep-purified platelets, and incubated them in EV-depleted blood plasma from healthy subjects and from patients with rheumatoid arthritis. EVs were subjected to differential centrifugation, size exclusion chromatography, or density gradient ultracentrifugation followed by mass spectrometry. Plasma protein-coated EVs had a higher density compared to the nascent ones and carried numerous newly associated proteins. Interactions between plasma proteins and EVs were confirmed by confocal microscopy, capillary Western immunoassay, immune electron microscopy and flow cytometry. We identified nine shared EV corona proteins (ApoA1, ApoB, ApoC3, ApoE, complement factors 3 and 4B, fibrinogen α-chain, immunoglobulin heavy constant $\gamma 2$ and $\gamma 4$ chains), which appear to be common corona proteins among EVs, viruses and artificial nanoparticles in blood plasma. An unexpected finding of this study was the high overlap of the composition of the protein corona with blood plasma protein aggregates. This is explained by our finding that besides a diffuse, patchy protein corona, large protein aggregates also associate with the surface of EVs. However, while EVs with an external plasma protein cargo induced an increased expression of TNF-α, IL-6, CD83, CD86 and HLA-DR of human monocyte-derived dendritic cells, EV-free protein aggregates had no effect. In conclusion, our data may

MSCA-ITN-2017-722148 TRAIN EV; Hungarian Academy of Sciences: János Bolyai Research Scholarship and "Momentum", Grant/Award Number: LP2016-4/2016; European Research Council, Grant/Award Numbers: ERC-CoG 724994, H2020-ITN-2018-813294-ENTRAIN; EU's Horizon 2020 research and innovation program, Grant/Award Number: 739593

shed new light on the origin of the commonly reported plasma protein 'contamination' of EV preparations and may add a new perspective to EV research.

KEYWORDS
aggregation, blood plasma, extracellular vesicles, mass spectrometry, protein corona

1 | INTRODUCTION

Extracellular vesicles (EVs) are membrane-enclosed structures that are released by cells either via membrane budding or via the exocytosis of multivesicular bodies (Buzas *et al.*, 2014; György *et al.*, 2011). EVs maintain cellular and body homeostasis. They participate in intercellular communication and control various processes such as blood clotting, immune function and tumorigenesis (György *et al.*, 2011). How EVs exactly exert their effect has been the subject of intensive research and much attention has been paid to the variety of cargo molecules that EVs carry including proteins or nucleic acids (Cvjetkovic *et al.*, 2016; Kowal *et al.*, 2016; Valadi *et al.*, 2007). Much of the EV cargo is located inside the vesicles. However, surface interactions of EVs may regulate their organo- and cellular tropism, immune recognition, and cellular uptake (Buzás *et al.*, 2018). The surface molecules of EVs such as tetraspanins are extensively used as markers of EVs (Théry *et al.*, 2018). However, besides these canonical exofacial molecules, the association of EVs with proteins of the extracellular matrix, complement system, immunoglobulins, coagulation factors, lipoproteins, nucleic acids and thiol-reactive antioxidants have been analysed in different studies (Buzás *et al.*, 2018). In light of this, MISEV2018 drives the attention to the need of distinguishing the topology of EV components (Théry *et al.*, 2018).

Despite surface molecules and surface interactions have a fundamental influence on the function of EVs, until now only sporadic pieces of experimental data have been available about EV surface interactions with proteins, lipoproteins or nucleic acids (Németh *et al.*, 2017; Sódar *et al.*, 2016). The present study was inspired by the increasing number of studies, which have demonstrated the association of EVs with specific molecules from blood (Baranyai *et al.*, 2015; György *et al.*, 2012; Karimi *et al.*, 2018; Onódi *et al.*, 2018). In line with this, protein lists of EVs in EV databases such as EVpedia (Kim *et al.*, 2013) or Vesiclepedia (Kalra *et al.*, 2012) show strikingly high number of plasma proteins in EV preparations. The consensus MISEV2018 guidelines recommend authors to look for common protein contaminants (such as albumin) in their EV preparations (Théry *et al.*, 2018). Here we asked the question if these proteins were contaminants or inherent components of EVs.

To answer this question, we analysed medium sized EVs (mEVs, with 100–800 nm diameter, typically sedimented at 10,000–20,000 g) in blood plasma (Lötvall *et al.*, 2014). Besides finding evidence for the formation of the vesicular protein corona, our work also sheds light on the unexpected dimensions of the surface interactome of EVs.

2 | MATERIALS AND METHODS

2.1 | Supporting information

Figure 1 shows the summarized work-flow of this study. Experimental details including types of rotors, antibodies and TaqMan assays used in this study are summarized in Tables S1–S3. We have submitted all relevant data of our experiments to the EV-TRACK knowledgebase (EV-TRACK ID: EV200102) (Van Deun *et al.*, 2017). The mass spectrometry (MS) proteomics data have been deposited to the ProteomeXchange Consortium via the PRIDE (Perez-Riverol *et al.*, 2019) partner repository with the dataset identifier PXD020584. MS datasets are also available in the Dataset S1.

2.2 | Sample collection and subjects

Ethics permission was obtained from the Hungarian Ministry of Human Capacities (EMMI) in agreement with the Hungarian Scientific and Research Ethics Committee (ETT TUKEB). Informed consent was given by all subjects involved in our studies. Altogether, 17 patients with rheumatoid arthritis (RA), with age of 58.8±16.5 years (mean±SD; range: 26–84 years; two males, 15 females) were involved in this study. The patients were treated at the Department of Rheumatology & Clinical Immunology, Semmelweis University (Budapest, Hungary). The median DAS28 (Disease Activity Score) of RA patients was 3.45 (range: 0.4–6.26) and the median CRP value was 8.74 mg/L (range: 0.48–30.53 mg/L). Only RA patients diagnosed on the basis of the American College of Rheumatology criteria were included (Aletaha *et al.*, 2010). The age of the 20 healthy subjects (HS) was 34.8±10 years (mean±SD; range: 25–62; three males, 17 females). Only people without any known history of diseases were included into the HS group. Smoking was not a criterion of exclusion. More detailed information about the enrolled subjects is found in Table S4 and S5.

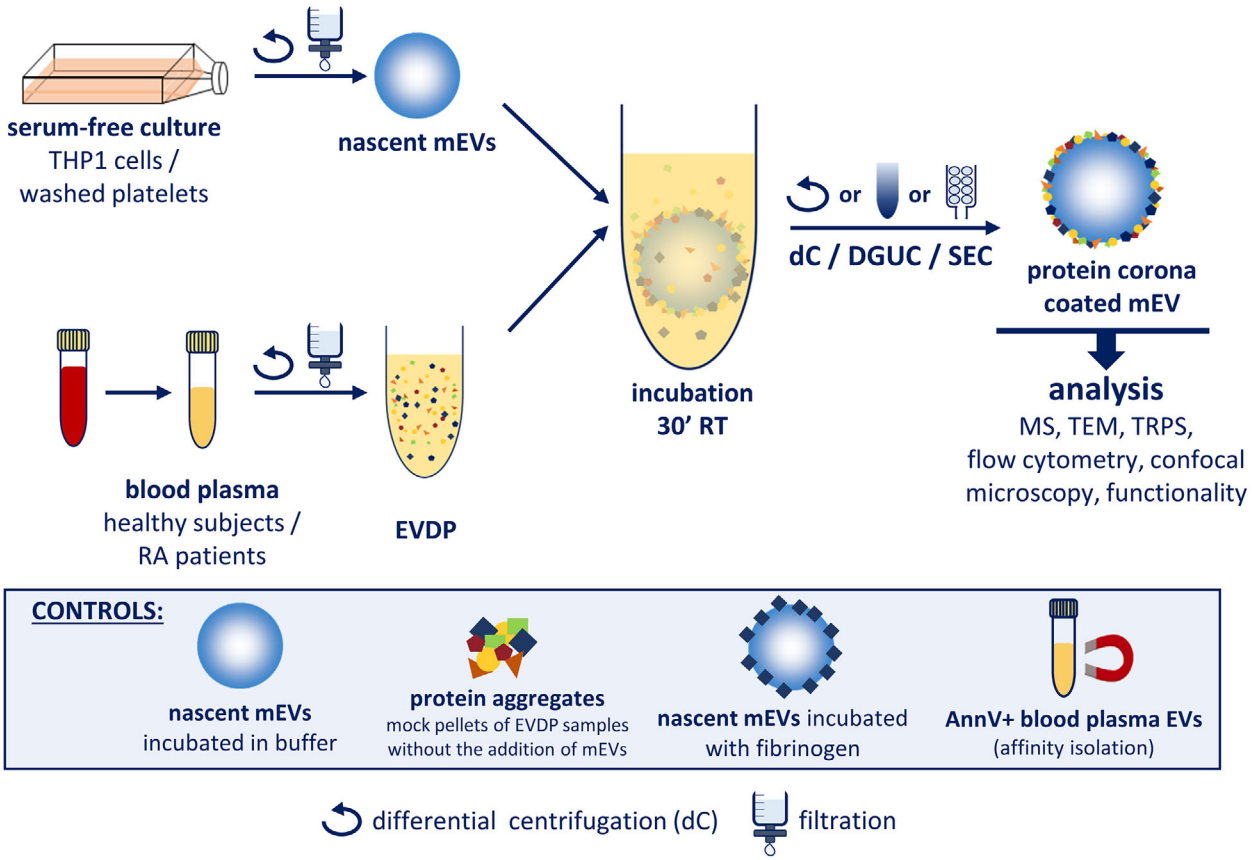

FIGURE 1 Schematic illustration of the work-flow. AnnV: Annexin V; dC: differential centrifugation; DGUC: density gradient ultracentrifugation; EVDP: extracellular vesicle-depleted blood plasma; mEV: medium sized extracellular vesicle; MS: mass spectrometry; RA: rheumatoid arthritis; RT: room temperature; SEC: size exclusion chromatography; TEM: transmission electron microscopy; TRPS: Tunable Resistive Pulse Sensing

Peripheral blood samples (18 mL/person) were collected from the cubital vein of healthy subjects and from patients with RA in acid-citrate-dextrose (ACD-A) tubes (Grenier). This anticoagulant tube was used to prevent in vitro release of EVs by platelets and blood cells (György *et al.*, 2014). It was not feasible to obtain fasting blood samples from RA patients and therefore, we collected non-fasting blood samples from healthy subjects as well. Blood was kept at room temperature and was processed within 3 h after collection.

2.3 | Production of EV-depleted blood plasma (EVDP) samples

Blood was centrifuged twice at 2500 g at RT for 15 min according to the recommendation of the International Society on Thrombosis and Haemostasis to yield platelet-free plasma (PFP) (Lacroix *et al.*, 2013). After the second centrifugation, all plasma samples were tested for the absence platelets using a Sysmex XE-2100 laboratory instrument, and the plasma was diluted two folds with 0.2 μm filtered phosphate buffered saline (PBS). Production of EV-depleted blood plasma (EVDP) samples was carried out as described previously (Aswad *et al.*, 2016; Eitan *et al.*, 2015; Liao *et al.*, 2017; Shelke *et al.*, 2014). Briefly, gravitation driven filtration was applied first with 5 μm and then with 0.8 μm filters. Next, the plasma was centrifuged at 20,000 g at 16°C for 40 min, and then the supernatant was ultracentrifuged at 100,000 g at 4°C for 16 h. The supernatant (EVDP) was aliquoted and stored at -80°C. Depletion in mEVs was confirmed by flow cytometry using Annexin V-FITC (fluorescein isothiocyanate, SONY) staining and by transmission electron microscopy (TEM) of the washed EVDP pellets obtained by 12,500 g centrifugation.

2.4 | Cell culture and isolation of platelets from platelet concentrates

THP1 monocytic cell line (ATCC) was cultured at 2.5–5 $\times 10^5$/mL concentration in RPMI 1640 medium (Sigma) containing 10% FBS (Gibco, BioSera), 1% Antibiotic Antimycotic Solution for Cell Culture (EMD Millipore) and 1% glutamine (Gibco).

Platelet concentrates were purchased from the Hungarian National Blood Transfusion Service on the day of their expiration. Platelets were isolated as described earlier (Aatonen *et al.*, 2014). Five mL of calcium- and magnesium-free Hanks' Balanced Salt Solution (HBSS, Sigma) and 5 μL of 1 μg/μL prostaglandin E1 (PGE1) solutions were added to 40 mL platelet concentrate. Samples were centrifuged at 900 g at RT for 15 min with slow acceleration and deceleration. The pellet was re-suspended in 15 mL HBSS, to which 100 ng/mL PGE1 solution was added. Next, 10–17% discontinuous iodixanol gradient (Optiprep, Sigma) was prepared in 50 mL Falcon tubes with the following layers: 13 mL 17%, 12 mL 13%, 12 mL 10%. Subsequently, 10–12.5 mL platelet suspension was layered onto the gradient. Tubes were centrifuged at 300 g at RT for 30 min. The middle layer, rich in platelets, was washed again at 300 g at RT for 5 min. The supernatant was centrifuged at 2200 g at RT for 15 min, after which the pellet was re-suspended in 100 mL calcium- and magnesium-free HBSS. Centrifugation was repeated, and the pellet was re-suspended in HBSS containing calcium and magnesium. The final concentration was 3×10^{11} platelet/mL.

2.5 | Nascent medium sized EV (mEV) isolation from cell culture

Nascents mEVs were harvested from serum-free conditioned media of THP1 cells. Cells were transferred into serum-free medium for 18–20 h at 5–10 $\times$ 10^5/mL concentration. The viability of cells was $\geq$ 90–95% (assessed by Annexin V-FITC binding by flow cytometry). Cells were centrifuged twice at 300 g at RT for 10 min. The pellet was discarded and the supernatant was transferred into new tubes each time. The supernatant was then filtered through a 5 μm filter (Millipore), was centrifuged at 2,000 g at 18°C for 20 min and was filtered again through a 0.8 μm filter (Millipore). The flow-through was then centrifuged at 12,500 g at 16°C for 40 min as described previously (Németh *et al.*, 2017; Visnovitz *et al.*, 2019). The supernatant was removed with a needle and syringe, and the pellet was washed once in 0.2 μm filtered (Millipore) 10 mM HEPES containing 0.9% NaCl, pH 7.4 ('EV buffer'). Again, the supernatant was removed with a needle and syringe, and the pellet was re-suspended in 130 μL EV buffer. Ten μL was kept frozen at -80°C for later bicinchoninic acid (BCA) protein measurements (Micro BCA Protein Assay Kit, Thermo Fisher Scientific), while the rest was used for incubation in (i) EVDP samples, or (ii) EV buffer (see below).

2.6 | Labelling THP1 cells with a lipophilic fluorescent dye (Vybrant DiO)

Prior to mEV isolation, THP1 cells were cultured as described above with the additional step of fluorescent labelling of the cellular membranes. One μL of DiO (Vybrant Multicolor Cell-Labelling Kit, Thermo Fisher Scientific) was added per 1×10^6 cells in 100 μL serum-free cell culture medium. After incubating for 20 min on 37°C, the cells were washed once in cell culture medium supplemented with 10% FBS, then twice with serum-free medium. Cells were then kept overnight in serum-free medium, and EV isolation was done as described above.

2.7 | Isolation of platelet-derived mEVs

Isolated platelets were incubated for 180 min at 37°C, 5% CO_2 with continuous gentle agitation. Subsequently, samples were centrifuged in two steps: first at 4750 g at RT for 5 min, then at 11,000 g at RT for 1 min. The supernatant was centrifuged again at 2500 g at RT for 15 min. After filtration of the supernatant through 0.8 μm filters, it was centrifuged at 20,000 g at 14°C for 40 min. The pellet was re-suspended in EV buffer and was washed once. Samples were then aliquoted and were stored at -80°C after snap freezing in liquid nitrogen.

2.8 | Incubation of nascent mEV preparations in human blood plasma samples

THP1 mEVs were separated from the conditioned medium of 8×10^7 cells (approximately 0.1 mg/mL protein concentration). The EVs were added in 60 μL to 500 μL EVDP samples from either healthy or from RA patients (Figure 1). As controls, we used either 60 μL of nascent mEV suspension in 500 μL EV buffer ('nascent EV only') or 60 μL buffer in 500 μL EVDP ('EVDP'). To exclude the possibility of missing EV proteins due to quantitative limitations of the samples, for the 'nascent mEV' samples, after the two washing steps, we tested at least one order of magnitude more concentrated nascent mEVs as well. Samples were incubated at RT for 30 min with rotation at slow speed (Fisherbrand Mini Tube Rotator, 10 rpm), and then we re-isolated the mEVs using three different approaches: (i) differential centrifugation (dC), (ii) density gradient ultracentrifugation (DGUC), and (iii) size exclusion chromatography (SEC) (see below). Nascent mEVs from Optiprep-purified platelets were incubated in

healthy EVDP samples ($n = 3$) in the same way as were nascent THP1 mEVs. The amount of platelet mEVs was matched to THP1 mEVs based on protein concentration. We re-isolated platelet-derived mEVs by dC.

2.9 | Re-isolation of mEVs via three different methods

2.9.1 | Differential centrifugation (dC)

In most cases, re-pelleting of mEVs was carried out by dC. Nascent mEVs were incubated in EVDP samples, after which they were washed twice with EV buffer at 12,500 g 40 min. In the case of platelet EVs ($n = 3$), the washing steps were performed with 20,000 g pelleting (Aatonen *et al*., 2014). For MS, the final pellet ($n = 12$ HS, $n = 10$ RA) was re-suspended in 30 μL high-performance liquid chromatography (HPLC) clean distilled water from which 10 μL was kept frozen for later Micro BCA-protein measurements, and 20 μL was used for MS. For other experiments, the pellet was re-suspended in EV buffer unless stated differently.

2.9.2 | Density gradient ultracentrifugation (DGUC)

Re-isolation of THP1 mEVs was also carried out by DGUC. A discontinuous iodixanol (Optiprep™) gradient was used as described earlier by Van Deun *et al.* (Van Deun *et al*., 2014) modified for the total volume of 4 mL of gradient (1 mL of 40%, 1 mL of 20%, 1 mL of 10% and 1 mL of 5% solutions layered onto each other in an 5 mL). Nascent mEVs incubated in healthy EVDP samples ($n = 3$) were loaded onto the top of the gradient in an open top 5 mL maximum volume polyallomer tube (Beckman Coulter). The samples were spun at 100,000 g on 4°C for 18 h (MLS-50 swinging-bucket rotor, Beckman Coulter, acceleration: nine, deceleration: coast). Fractions of 500 μL were collected starting from the top of the gradient, and the density of each fraction was determined by measuring the weight of identical volume of each sample. Each fraction was diluted to 2 mL with EV buffer, from which 30 μL was separated for flow cytometry, while the rest was centrifuged at 12,500 g at 16°C for 80 min. The supernatant was then removed using a needle and syringe, and the pellets were re-suspended in 20 μL of HPLC distilled water. Meanwhile, flow cytometry analysis of each sample was carried out and those two or three fractions where Annexin V-FITC positive EVs were detected, were pooled and were then analysed by MS. The number of Annexin V-FITC positive vesicles in the different fractions was also determined. The representative TEM image of the re-isolated coated mEVs can be found as Figure S1(A).

2.9.3 | Size exclusion chromatography (SEC)

Besides using DGUC, aliquots of the same HS samples ($n = 3$) were also separated by SEC. Size exclusion columns (qEVoriginal (IZON), separation size: 70 nm nominal, bed volume 10 mL) were used according to the instructions of the manufacturer. As elution buffer, EV buffer was used after performing the recommended column equilibration. We pooled 1–3, 4–6, 7–9 and 10–12 fractions (1,500 μL/each pool) and were analysed by flow cytometry. Only fractions 7–9 contained Annexin V-FITC positive, Triton-sensitive events (Triton X-100, 0.1%). The pooled fractions were then spun at 12,500 g at 16°C for 40 min, the pellets were re-suspended in 20 μL of HPLC distilled water and were subjected to MS analysis. The representative TEM image of the re-isolated coated mEVs can be found as Figure S1(B).

2.10 | Isolation of blood plasma mEVs based on Annexin V affinity capture

Platelet-free plasma samples (from 18 mL ACD-A anticoagulated blood/person) of three HSs were pelleted at 20,000 g, 40 min, 16°C, after which the supernatants were removed carefully with a needle and syringe. The pellets were then re-suspended in 300 μL Annexin-binding buffer (ABB) (BD Pharmingen). Meanwhile, 10 μL of Streptavidin MicroBeads (MACS, Miltenyi Biotec) was incubated with 10 μL Annexin V MicroBeads (MACS, Miltenyi Biotec) per sample for 30 min at RT, with low-speed rotation (Fisherbrand Mini Tube Rotator, 10 rpm). Beads were then transferred into the blood plasma mEV samples (20 μL of the mixed beads into each sample) and were incubated for 60 min at RT, with low-speed rotation. Samples were then loaded onto μ Columns (MACS, Miltenyi Biotec) that were previously equilibrated with 0.1% Triton X-100 and washed four times with ABB. Columns were then washed six times with ABB. Samples were eluted with 100 μL protein lysis buffer (Raybiotech Inc.). Protease inhibitors were added to the samples (protease inhibitor cocktail (Sigma), 0.005 M phenylmethylsulphonyl fluoride (PMSF, Sigma), 0.001 M sodium orthovandate (Sigma)), after which samples were frozen-thawed three times and sonicated for 20 min. Protein concentration was determined with a Micro BCA assay. Samples were then kept frozen at -20°C till they were used for Wes analysis.

2.11 | Mass spectrometry (MS)

Medium sized EV samples were prepared as described above and stored frozen at -80°C in 20 μL HPLC clean distilled water. Proteins were extracted by repeated freeze-thaw cycles and digested by a miniaturized tryptic digestion protocol as described earlier (Turiák *et al.*, 2011). Samples were analysed on a Dionex Ultimate 3000 nanoRSLC (Dionex) coupled to a Bruker Maxis II mass spectrometer (Bruker Daltonics GmbH) via CaptiveSpray nanobooster ionsource. Peptides were separated on an ACQUITY UPLC M-Class Peptide BEH C18 column (130 Å, 1.7 μm, 75 μm x 250 mm, Waters, Milford, MA, USA) following trapping on an Acclaim PepMap100 C18 NanoTrap column (100 Å, 5 μm, 100 μm × 20 mm, Thermo Fisher Scientific). Data dependent analysis was performed using a fix cycle time of 2.5 s. Raw data files were processed using the Compass DataAnalysis software (Bruker). Protein identification was performed utilising search engines Mascot (Matrix Science, version Mascot 2.5) and X!Tandem (The GPM, thegpm.org; version 2007.01.01.1) against the Swissprot *Homo sapiens* database (2015_08). The following search criteria were used: 10 ppm peptide mass tolerance, 0.15 Da fragment mass tolerance and two missed cleavages. Carbamidomethylation on cysteines was set as fixed modification and the following variable modifications were applied: deamidation (N, Q), and oxidation (M). Data were analysed with the help of FunRich (Pathan *et al.*, 2015; Pathan *et al.*, 2017) and Scaffold 4.5.3 (http://www.proteomesoftware.com) programs. Keratins and other skin proteins (e.g., hornerin, desmoplakin, dermicidin and desmoglein) were omitted from the final protein lists as potential contaminants.

2.12 | Tunable resistive pulse sensing (TRPS)

Nascent THP1 mEVs, coated EV samples (incubated in healthy EVDP), and pellets of the same EVDP samples without the addition of nascent mEVs were produced by dC and were analysed by TRPS using a qNano instrument (IZON) as described previously (György *et al.,* 2014; Osteikoetxea *et al.*, 2015; Osteikoetxea *et al.*, 2015; Szabó *et al.*, 2014) ($n = 3$). An NP400 nanopore membrane (IZON) stretched between 43 and 47 mm was utilized for the measurements. Voltage was set to 0.04–0.7 V to achieve a stable current, while the applied pressure was set to 5–10 mbar. Samples were also analysed after 0.1% Triton X-100 lysis. The analysis of each sample was stopped after counting at least 500 particles or, in the case of very low particle concentration, after 5 min. For calibration, we used calibration beads (200 nm) according to the instructions of the manufacturer (IZON). Detailed results of measurements are available in Table S6.

2.13 | Nanoparticle tracking analysis (NTA)

A ZetaView Z-NTA instrument (ParticleMetrix) with a ZetaView Analyze 8.05.10 software was used for the comparison of size distribution of THP1 and platelet-derived nascent mEVs from Optiprep-purified platelets (separated by 12,500 g and 20,000 g centrifugations, respectively). For sample dilution, EV buffer was used with 15,000.00 μS/cm conductivity. The used laser wavelength was 520 nm. The measurement mode was size distribution with two cycles. The camera settings were the following: auto expose, sensitivity: 80, shutter: 100, gain: 28.8, offset: 0, while the analysis parameters were: max area: 10,000, min area: 5, min brightness: 20. Measurement temperature was 25°C. Each sample was measured in three technical replicates. Results are shown in Figure S2 and Table S7.

2.14 | Transmission electron microscopy (TEM)

2.14.1 | Immune EM

Coated THP1 mEVs were produced by incubation of nascent mEVs in healthy EVDP samples and were isolated with dC as detailed above. The 12,500 g pellet was re-suspended (after the second washing step) in 10 μL EV buffer, was snap frozen and was stored at -80°C. Samples were thawed up at RT before use. In all cases, nascent mEVs and pellets of EVDP samples were used as controls.

Immune EM was carried out as we described previously (Visnovitz *et al.*, 2019). Briefly, 2 μL sample was carefully pipetted on a nickel grid. Samples were dried for 10 min at RT. They were then fixed with 4% paraformaldehyde (PFA) for 10 min and were washed three-times with 0.2 μm filtered PBS. Blocking was then carried out with 5%, 0.2 μm filtered bovine serum albumin (BSA in PBS) for 1 h at RT. Samples were then stained with primary antibodies specific for different proteins (anti-human, mouse or rabbit antibodies diluted 5–50 fold depending on the stock concentration: polyclonal fibrinogen antibody produced in rabbits (Bioss); polyclonal complement C3 antibody produced in rabbits (Thermo Fisher Scientific), polyclonal haptoglobin antibody

produced in rabbits (Thermo Fisher Scientific), monoclonal ApoA1 antibody, produced in mice (Thermo Fisher Scientific), monoclonal CD63 antibody produced in mice (SONY)). The detailed specification of antibodies used in this study is included in Table S2. Samples were stored overnight at 4°C. On the next day, washing with 0.2 μm filtered 5% BSA was carried out three times for 5 min, and then staining with 50x diluted secondary antibodies (goat polyclonal IgG anti-rabbit antibody, conjugated with 10 nm gold particles (Abcam); goat polyclonal anti-mouse IgG antibody, conjugated with 5 nm gold particles (Sigma)) was applied for 180 min at RT. Samples were washed twice with 0.2 μm filtered 5% BSA for 5 min each time, after which washing with PBS and then with distilled water was performed. Samples were fixed with 2% glutaraldehyde for 10 min at RT, washed with distilled water for 5 min three times and then were stained with phosphotungstic acid at RT for 15 min. Washing was then repeated three times, after which grids were dried and stored until examination with transmission EM (JEOL 1011 transmission electron microscope (Japan)).

2.14.2 | Ultrathin sections without immunogold labelling

The embedded and ultrathin sectioned samples, analysed by transmission EM were as follows: (1). nascent THP1 mEVs incubated (i) in 1 mg/mL fibrinogen (Sigma), or (ii) in EV buffer for 30 min at RT. EVs were then pelleted by centrifugation at 12,500 g at 16°C for 40 min. (2). nascent THP1 mEVs incubated in healthy EVDP samples for 30 min at RT and then pelleted by DGUC. (3). nascent THP1 mEVs incubated as in 2 and isolated by SEC. The pellets were fixed with 2% glutaraldehyde and 2% PFA (both obtained from Sigma). The embedding and TEM procedures were carried out as described previously (Németh *et al.*, 2017).

2.15 | Confocal microscopy

The serum free conditioned medium of DiO-stained (Thermo Fisher Scientific, as described earlier) THP1 cells was collected after 18 h. mEVs were separated by dC and nascent and HS EVDP-coated THP1 mEVs were immuno-stained with primary antibodies including monoclonal fibrinogen α-chain antibody produced in mice, polyclonal complement C3 antibody produced in rabbits (from Thermo Fisher Scientific). Alexa647 and Alexa594 donkey secondary antibodies were used. Secondary antibody controls (without the addition of primary antibodies) and a DiO dye control were used. Images of secondary antibody controls are provided as Figure S3(A–D). DiO dye control gave no detectable signal. Twenty μL of the immuno-stained nascent or HS EVDP-coated mEV suspensions were dried on the surface of gelatine-coated glass slides. Dried droplets were mounted with Aqua-Poly/Mount medium (Polysciences, USA). EVs were analysed using a Nikon Eclipse Ti-E inverted microscope (Nikon Instruments Europe B.V., Amsterdam, The Netherlands), with a CFI Plan Apochromat VC 60XH oil immersion objective (numerical aperture: 1.4) and an A1R laser confocal system. We used 488, 561 and 647 nm lasers (CVI Melles Griot), and scanning was done in line serial mode. Image stacks were obtained with NIS-Elements AR software.

2.16 | Determination of protein and lipid concentrations in serially centrifuged EVDP samples

The serial centrifugation of healthy EVDP samples ($n = 3$) was performed as follows: 500 μL EVDP sample was spun after the addition of 1 mL of EV buffer at 12,500 g at 16°C for 40 min. After each round of centrifugation, the supernatant was removed carefully by a needle (16G) and a syringe, and was transferred to a new tube, while the pellet was washed once with 1 mL EV buffer. The samples were centrifuged 6 consecutive times. The washed pellets after each run were re-suspended in HPLC distilled water, and were subjected to lipid and protein concentration analysis. Lipid concentration was determined using the improved 96-well plate format lipid quantification sulfo-phospho-vanillin (SPV) assay (Visnovitz *et al.*, 2019), while the protein concentration of the samples was measured with a Micro BCA assay.

2.17 | Exposure of dendritic cells to nascent and coated EVs as well as protein aggregates

2.17.1 | Human monocyte-derived dendritic cell (moDC) cultures

Leukocyte-enriched buffy coats were obtained from healthy blood donors drawn at the Regional Blood Centre of the Hungarian National Blood Transfusion Service (Debrecen, Hungary) in accordance with the written approval of the Director of the National Blood Transfusion Service of the University of Debrecen, Faculty of Medicine (Hungary) and from the Regional and Institutional Research Ethical Committee of the University of Debrecen. Peripheral blood mononuclear cells (PBMCs)

were separated by a standard density gradient centrifugation with Ficoll-Paque Plus (Amersham Biosciences). Monocytes were purified from PBMCs by positive selection using immuno-magnetic cell separation and anti-CD14 microbeads, according to the instructions of the manufacturer (MiltenyiBiotec). After separation on a VarioMACS magnet, 96–99% of the cells were CD14+ monocytes, as measured by flow cytometry. Isolated monocytes were plated at 1×10^6 cell/mL concentration in AIM-V medium (Gibco) containing L-glutamine and supplemented with 1% Gentamicin/Streptomycin solution (Hyclone) in the presence of 100 ng/mL IL-4 (Peprotech EC) and 80 ng/mL GM-CSF (Gentaur Molecular Products) On day 2, the same amounts of IL-4 and GM-CSF were added to the cell cultures. Monocytes were cultured for 5 days in 24-well tissue culture plates.

2.17.2 | Exposure of moDCs to THP1 mEVs with/without coating or to pellets of EVDPs

Nascent THP1 mEVs were isolated and incubated in either healthy or RA EVDP samples as described above. Thirty μL nascent mEV preparation produced by 4×10^6 THP1 cells was incubated in 250 μL EVDP. Re-isolation and washing of vesicles were carried out by dC at 12,500 g at 16°C for 40 min. As controls, pellets of nascent mEVs incubated in EV buffer and pellets of EVDP samples were also produced. The final pellets were re-suspended in 50 μL EV buffer and were carefully added to the culture media of cells. Cells were exposed to the pellets for 48 h, after which flow cytometry of cells and enzyme-linked immuno-sorbent assay (ELISA) of the conditioned media were performed. As controls, we used unstimulated cells to which EV buffer was added to the cells (instead of a pellet).

2.18 | Exposure of human peripheral blood cells to DiO-stained THP1-derived mEVs with/without coating

Three mL peripheral venous blood was drawn into EDTA (ethylenediaminetetraacetic acid) anticoagulant blood collection tubes (Greiner) from healthy subjects ($n = 3$). Sixty μL blood was transferred into flow cytometry tubes in three replicates. One mL lysis buffer (5% diethylene glycol, 1.5% formaldehyde, 0.25% sodium citrate and 0.1% sodium heparin (all from Sigma) in distilled water) was added to lyse red blood cells and after 10 min incubation on RT, samples were washed twice with PBS. Next, cells were re-suspended in 300 μL RPMI and were exposed to either (i) EV-buffer, (ii) nascent Dio-stained-THP1 mEVs, and (iii) HS EVDP coated Dio-stained-THP1 mEVs isolated with dC. The number of nascent and coated THP1 mEVs was determined with flow cytometry and approximately 650,000 mEVs were added to each sample. Cells were incubated for 45 min at 37°C, were washed once with PBS, and were fixed with 2% PFA after which they were analysed by flow cytometry.

2.19 | Flow Cytometry

Flow cytometric detection of the mEVs was carried out with a FACS Calibur Flow Cytometer (van der Pol *et al.*, 2018). The vesicular gate was set using Megamix Beads (Biocytex; 160 nm, 200 nm, 240 nm and 500 nm). Gate setting was optimized with 1 μm Silica Beads Fluo-Green (from Kisker) as described previously (Sódar *et al.*, 2016). For the detection of mEVs, Annexin V-FITC staining was used. Dye-only and unstained controls were also tested. For the determination of the vesicle concentration, count check beads were applied (Sysmex, 104,890 beads/m*L*, or 249,900 beads/m*L*). Lysis with 0.1% Triton was applied for 5–10 min to prove the vesicular nature of events (György *et al.*, 2011). To detect association of fibrinogen with mEV surface, 1 μL of ~1 mg/mL protein concentration nascent THP1 mEV samples were incubated in 300 μL of 1 μg/mL FITC-labelled fibrinogen (Abcam) for 30 min at RT and then were analysed by flow cytometry. Fibrinogen binding was also tested after high salt concentration washing (0.75 M or 1.5 M). In these cases, 100 μL of 2.25 M or 4.5 M NaCl solution was added to EVs in 200 μL EV buffer containing fibrinogen, after which flow cytometry was performed as described above.

The binding of fibrinogen to THP1 cells was also tested. Cells (grown in a serum-free medium overnight) were washed once in EV buffer and were then incubated in the presence of 2 μg/mL FITC-labelled fibrinogen for 30 min at RT. After the incubation time, cells were washed once and their surface fluorescence was analysed by flow cytometry.

Additionally, moDCs stained with anti-human CD83-phycoerythrin (PE, BioLegend), HLA-DR-peridinin-chlorophyll-protein (PerCP) and CD86-allophycocyanin (APC) (both from BD Biosciences) were also analysed by flow cytometry. Fluorescence intensities were measured by a NovoCyte flow cytometer (ACEA Biosciences).

For analysing the DiO-stained THP1-derived mEV uptake, blood cell populations (lymphocytes, monocytes, neutrophils) were gated based on their forward- and side-scatter (FSC and SSC) properties and the threshold for DiO positivity was set based on the background of EV-buffer-treated cells. The percentage and the GeoMean of DiO positive cells were measured and compared between nascent and coated mEV-treated blood cells. For each measurement, 50,000 events/sample were counted.

2.20 | Measurement of cytokine concentrations by ELISA

Conditioned medium of moDCs was harvested 6 days after monocyte separation. The concentrations of IL-6 (BD Biosciences) and TNF-α (BD Biosciences) were measured by OptEIA kits (BD Biosciences) according to the instructions of the manufacturer.

2.21 | Quantitative PCR analysis of gene expression in THP1 cells

THP1 cells were grown in a serum-free medium for 20–22 h. Total RNA of cells was isolated with the Blood/Cell Total RNA Mini Kit (Geneaid) according to the instructions of the manufacturer. RNA concentration was determined by a NanoDrop instrument. Five hundred ng RNA was reverse transcribed to cDNA with SensiFAST cDNA Synthesis Kit (Bioline). Samples were then added to 96-well plates together with TaqMan Fast Advanced Master Mix (Thermo Fisher Scientific) and FAM TaqManGene Expression Assay primers (for genes: *hHPRT1, ALB, APOB, IGKC, TF*) in a total volume of 20 μL. The detailed specification of the TaqMan primers is summarized in Table S3. The reaction was carried out on an Applied Biosystems 7900HT Fast real-time PCR instrument. A Ct value cut-off $\leq$ 35 was considered as positive result.

2.22 | Capillary Western (Wes) analysis of blood plasma mEVs

Wes analysis was performed with a ProteinSimple-Biotechne 004–600 Wes system using a 12–230 kDa Separation Module (ProteinSimple) following the instructions of the manufacturer. Briefly, lysates of Annexin V-captured blood plasma mEVs were used in a 0.15 μg/μl concentration, were mixed with the Fluorescent Master Mix 1:4 and heated at 95°C for 5 min. Primary antibodies CD63 polyclonal antibody produced in rabbits, (SantaCruz), monoclonal fibrinogen α-chain antibody produced in mice, monoclonal antibody produced in rabbits (both from Bio-Techne R&D), polyclonal complement C3 antibody produced in rabbits, monoclonal ApoA1, produced in mice, polyclonal complement C4b antibody produced in rabbits, polyclonal ApoE antibody produced in rabbits (all from Thermo Fisher Scientific) were diluted 50-fold with the Antibody diluent two solution (ProteinSimple). Depending on the applied primary antibodies, horseradish peroxidase (HRP)-conjugated anti-rabbit (ProteinSimple) or anti-mouse secondary antibodies were applied (both produced in goats). The samples, blocking reagent (antibody diluent), primary and secondary antibodies, the chemiluminescent substrate (Peroxide and Luminol-S (both from ProteinSimple) and the wash buffer (Protein Simple) were loaded onto the plate. The settings of the system were as follows: separation load time: 200 s, stacking load time 15 s, sample load time 9 s, separation time 25 min, separation voltage 375 V, blocking reagent: 5 min, primary and secondary antibodies both for 30 min. Chemiluminescent detection profile was set for High Dynamic Range (HDR 4.0). Contrast was manually adjusted for each sample. Wes data and gel pictures were analysed using the software Compass for SW (Protein Simple).

2.23 | Bioinformatic tools and databases

Venn diagrams were drawn in Microsoft Power Point based on the analysis provided by either FunRich Functional Enrichment Analysis Tool (Pathan *et al.*, 2015; Pathan *et al.*, 2017), or by the online platform, InteractiVenn (Heberle *et al.*, 2015). Gene Enrichment Analysis was performed with FunRich. Flow cytometric data were analysed using the FlowJo vX.0.7. software (Tree Star). The Vesiclepedia database ((Kalra *et al.*, 2012), http://microvesicles.org) was used applying the 'Query' function of the site. Only *Homo sapiens* entries were included in our analysis, by the date 05.04.2020. Vesiclepedia generated a list of 'TOP 100 EV proteins', which included gene symbols for top hits regardless of the species of origin. For predicting protein-protein interactions, the online platform and database, STRING was used ((Szklarczyk *et al.*, 2019), https://string-db.org). The minimum required interaction score was set to 0.700 (high confidence). All interaction sources of the database (textmining, experiments, databases, co-expression, neighbourhood, gene fusion, co-occurrence) as well as both physical and functional protein associations were considered in the analysis. The network was then further analysed with Microsoft Excel and illustrated with the yEd Graph Editor. Graph centrality measures were set based on the number of connected edges to each node. Nascent THP1 mEV proteins with predicted membrane localisation were identified using the UniProt database (Bateman *et al.*, 2021). For comparative *in silico* analysis of protein corona proteins of different viruses and artificial nanoparticles, we used proteomic data based on the datasets provided in the Supplemental material of the publication by Ezzat *et al.* (Ezzat *et al.*, 2019). Only human proteins identified by the authors in viruses or in lipid nanoparticles incubated in human plasma samples were included in our analysis. We subtracted proteins that were also present in the 'virus only' samples, from the final protein lists. From our own data, in the analysis we included only those proteins that could be detected in $\geq$ 30% of our dC obtained coated vesicle samples.

2.24 | Statistics

Numerical data were evaluated in Microsoft Excel. Statistics were carried out with the GraphPad Prism 8 software (GraphPad Software Inc.). Normality of data was determined prior to analysis with D'Agostino & Pearson test or when the number of data elements was too low to perform this test, with Shapiro-Wilk test. Student's t-test, Mann-Whitney U test, Kruskal-Wallis test with Dunn's post-test and one-way ANOVA test with Tukey's post-test were used according to the distribution of the data with $^{*}P < 0.05$, $^{**}P < 0.01$, $^{***}P < 0.001$, and $^{****}P < 0.0001$ significance levels.

3 | RESULTS

3.1 | Identification of proteins associated with nascent THP1-derived or Optiprep-purified platelet-derived mEVs after incubation in blood plasma

As shown in Figure 1, nascent THP1 mEVs (harvested from serum free conditioned medium) were incubated either in healthy subject (HS) or rheumatoid arthritis (RA) patient-derived EVDP samples. After the incubation period, mEVs were isolated again (either with dC as a first screen ($n = 22$), or with DGUC (HS, $n = 3$) or with SEC (HS, $n = 3$). The mEVs were washed twice before subjecting them to MS analysis. Nascent mEVs pre-incubated in buffer instead of EVDP were also included in the analysis. The list of proteins found in an at least one order of magnitude higher concentration nascent mEV sample (as compared to those used for incubation in EVDPs) was subtracted from the protein lists of the individual coated mEV samples. The results of the subtraction yielded a list of proteins we named 'protein corona'. In the next step, we determined the percentage in which a protein was detected among all samples. Altogether 61 proteins were identified in ≥ 30% (an arbitrarily selected limit) of all the 22 protein-coated THP1 mEV preparations isolated with dC (Figure 2). Forty-two proteins out of them were equally abundant in healthy and RA samples while 16 proteins were preferentially associated with RA (found at least 1.5-fold more frequently in the RA coronas than in the healthy ones) (Figure 2). Twenty proteins were found in ≥ 90% of all samples. The highest number of proteins was detected in dC preparations as compared to preparations gained by DGUC or SEC (Figure 2). Of note, in this work we made an attempt to avoid centrifugation as much as possible, and therefore, we loaded diluted platelet free plasma samples on the columns. SEC resulted in further dilution of the samples. Therefore, we identified an overall lower number of proteins in the SEC samples, and this was also true for the DGUC samples. A tabulated list of proteins shown in this figure is provided in Table S8. Interestingly, we identified several proteins ($n = 66$), such as albumin both in nascent THP1 mEV preparations as well as in ≥ 30% of all EVDP-incubated mEV samples. The tabulated proteins list of these proteins is provided in Table S9. Therefore, by rule, these proteins were not included in the primary list of corona proteins. Nine of these proteins are known to have secreted forms according to UniProt (Bateman *et al.*, 2021)), we suggest that these proteins could be considered as members of an extended protein corona around mEVs. These proteins labelled with asterisks are shown in Figure 2(b).

We hypothesized that if there was a protein corona composed of the identified proteins around mEVs, it would be reflected by an increased mEV floatation density. Therefore, we subjected our nascent and protein corona coated mEVs to DGUC. In line with our expectations, EVDP-incubated mEVs had a higher density than the nascent ones; the percentage of nascent and coated EVs differed significantly in the 1.10 mg/ml and the 1.15 mg/ml fractions (multiple t-test, $P < 0.001$ and $P < 0.01$, respectively) (Figure 2c).

We also compared the protein coronas of THP1 mEVs and of mEVs from Optiprep-purified platelets (both separated by dC) and found a 44% overlap (Figure S4 and Table S10). In addition, we also compared the THP1 mEV corona proteins with those found in plasma-derived mEVs isolated with dC at 20,000 g. This comparison also showed a high overlap of proteins (53 out of the 61 THP1 mEV corona proteins were also present in these samples). These data are also provided as a tabulated protein list as Table S11.

Next, we set to compare the 61 proteins that we identified in ≥ 30% of protein-coated THP1 mEV preparations (isolated with dC) with components of the protein coronas formed around viruses (including herpes simplex virus (HSV) and respiratory syncytial virus (RSV)) and artificial lipid nanoparticles (LNPs). To this end, we re-analysed the only available published viral corona proteomic datasets of Ezzat *et al.* (Ezzat *et al.*, 2019). Importantly, we identified 9 shared corona proteins that could be detected in all protein coronas (around HSV, RSV, the positively and the negatively charged LNPs as well as our THP1- and platelet-derived mEVs). (Figure 3a). These included ApoA1, ApoB, ApoC3, ApoE, complement factor 3, complement factor 4B, fibrinogen α-chain, immunoglobulin heavy constant γ2 (IgG2) and immunoglobulin heavy constant γ4 (IgG4) chains. Although albumin is probably the best known extracellular protein in blood plasma EV preparations, and it was indeed present in all our MS datasets, here it is not listed among the primary core corona proteins because nascent mEV preparations also included it. Of note, we identified additional potential corona proteins which were absent from only one of the compared datasets (Figure 3a).

We also identified the nine shared corona proteins in the protein list of human blood plasma-derived mEVs obtained with dC at 20,000 g (HS, $n = 3$). Importantly these proteins were also present in the plasma mEVs isolated by Annexin V-based affinity

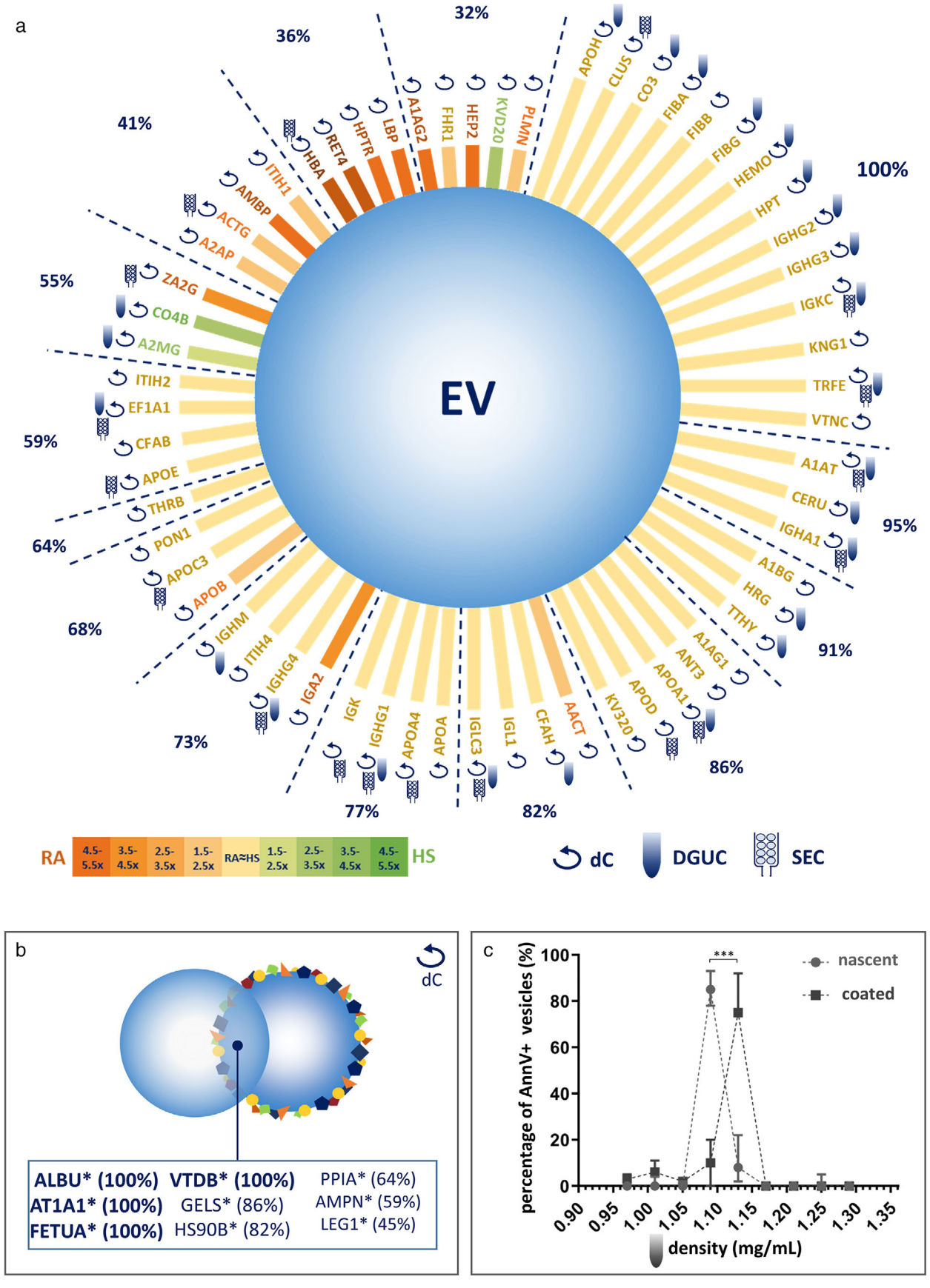

FIGURE 2 A protein corona is formed around nascent THP1 EVs upon incubation in blood plasma. (a): THP1 monocytes were cultured under serum free conditions, and nascent mEVs were isolated. These mEVs were next incubated in EV-depleted blood plasma (EVDP) samples from healthy subjects (HS)

capture (HS, $n = 4$; (Figure 3b-i). The figure shows shared corona components identified by a Wes system along with the EV-membrane protein CD63. (The complete gels are shown in Figure S5). The presence of these shared corona proteins in Annexin V-captured EVs provides evidence that these proteins are organic components of the protein corona.

We then searched the Vesiclepedia database (Kalra *et al.*, 2012) for entries matching our top corona proteins found in > 90% of our plasma protein-coated samples obtained with dC ($n = 20$) (Figure 3j). With a few exceptions, these corona proteins were present in at least 20 EV entries, and two of them (clusterin/ApoJ) and complement C3 protein) were found even in > 160 EV entries/protein. To our surprise, most of these proteomic data were obtained from the analysis of non-blood plasma-derived EV samples. Vesiclepedia provides the list of TOP100 proteins identified in EVs in submitted datasets. This list in fact contains gene symbols rather than protein IDs. Thus, in order to compare this list with our list of proteins, we harmonized the gene symbols with UNIprot_IDs (the term translation set of gene symbols to UniProt IDs can be found in Table S12). Given that gene symbols HIST4H4, HIST1H4A, HIST1H4B, HIST1H4D, HIST1H4F, HIST1H4H, HIST1H4I, HIST1H4J and HIST1H4K all corresponded to H4_HUMAN, the number of proteins of the harmonized 'TOP100 EV protein' list at the end contained only 92 proteins. The Venn diagram in Figure 3k shows the overlap among proteomic hits in Vesiclepedia 'TOP100 EV protein' entries, and proteins also present (i) in > 30% of proteins identified in both nascent THP1 mEV and coated THP1 mEV lists, and (ii) coated THP1 mEV samples as well as (iii) in > 30% of pellets of EVDP samples corresponding to protein aggregates. Out of the proteins that we identified in our nascent THP1 mEV samples, 72 matched the 'TOP100 EV proteins' of Vesiclepedia (Figure 3l).

FunRich gene enrichment analyser (Pathan *et al.*, 2015; Pathan *et al.*, 2017) identified the following biological processes with the highest percentages among the THP1 mEV-associated corona proteins: protein metabolism (34.8%), immune response (26.1%) and transport (26.1%) (Figure S6).

3.2 | Microscopic imaging of the protein corona around THP1 mEVs

Our confocal microscopy analysis revealed that some EVs were surrounded with a diffuse (patchy) protein corona whereas in other cases the corona was represented by an EV-surface attached large protein aggregates (Figure 4a-i panels).

Having identified numerous proteins associated with mEVs by MS, we addressed the question if these mEV-associated corona proteins could be identified by immunogold EM. Figure 5a shows a schematic illustration of our immunogold labelling approach. Fibrinogen alpha chain binding to EVs alone (Figure 5b) or in parallel with APOA1 (Figure 5c) were captured. Our immunogold labelling also revealed co-localization of (i) the EV membrane protein CD63 with haptoglobin (Figure 5d), (ii) CD63 with the C3 complement protein (Figure 5e), and (iii) haptoglobin and APOA1 (Figure 5f).

We also asked the question whether the presence or absence of protein corona had an impact on the TEM appearance of mEVs. To this end, we analysed ultrathin cross-sections of THP1 mEV preparations either in a nascent or protein-coated form. In preliminary experiments we found that in cross sectioned pellets of EVDP-coated mEVs the vesicular structure was obscured by the large amount of proteins. Therefore, to get a better visualization, we incubated our nascent THP1 mEVs with a single corona protein (fibrinogen) before the TEM analysis. As shown in Figure 6a, nascent mEVs were characterized by sharp membrane boundaries, whereas fibrinogen-coated mEV membranes had a 'fluffy' appearance (Figure 6b). With the analysis of 6 independent fields, in the case of nascent mEVs ($n = 596$ vesicles) and eight independent fields of coated mEVs ($n = 839$ vesicles), we found a significant difference in the number of 'fluffy' vesicles (t-test, $P < 0.0001$) (Figure 6c).

3.3 | Interactions of proteins associated with mEVs

We decided to carry out an analysis of protein-protein interactions of the corona components (i) with the THP1 mEV membrane proteins, and (ii) with other corona proteins. First, based on the UniProt database (Bateman *et al.*, 2021), proteins with predicted membrane localization were identified in the nascent THP1 mEV protein list. Next, we analysed the interactions of

and patients with rheumatoid arthritis (RA). Plasma-incubated mEVs were subsequently separated by differential centrifugation (dC) (HS, $n = 12$, RA $n = 10$), density gradient ultracentrifugation (DGUC) (HS, $n = 3$) or size exclusion chromatography (SEC) (HS, $n = 3$). The protein content of the re-isolated mEVs was analysed by MS. As controls, nascent mEVs were used. We identified 61 corona proteins, which were present in more than 30% of the plasma-coated THP1 mEV samples but not in nascent mEVs. A protein was considered to be preferentially found in RA plasma-coated THP1 mEV samples, if it was found at least 1.5-fold more frequently in the RA coronas than in the healthy ones. The proteins that could be identified by DGUC and/or SEC besides the standard dC are indicated by symbols next to the abbreviation of the name of each human protein. Protein name abbreviations are derived from the UniProt IDs of each protein, omitting the species of origin (_HUMAN). (b): The primary protein corona list (identified in dC samples) did not include some proteins due to their presence also in nascent mEVs. These proteins are considered as members of an extended protein corona list and are indicated with asterisk. Their frequency among all samples is indicated in the figure. (c): Flow cytometry analysis of Annexin V (AnnV) positive events in density gradient ultracentrifugation fractions of THP1 mEVs (either nascent ($n = 3$) or corona coated ($n = 3$)). The density of THP1-derived mEVs is shifted to a higher density upon incubation in EVDP samples prior to DGUC as compared to nascent mEVs. $P < 0.001$ and $P < 0.01$; multiple t-test

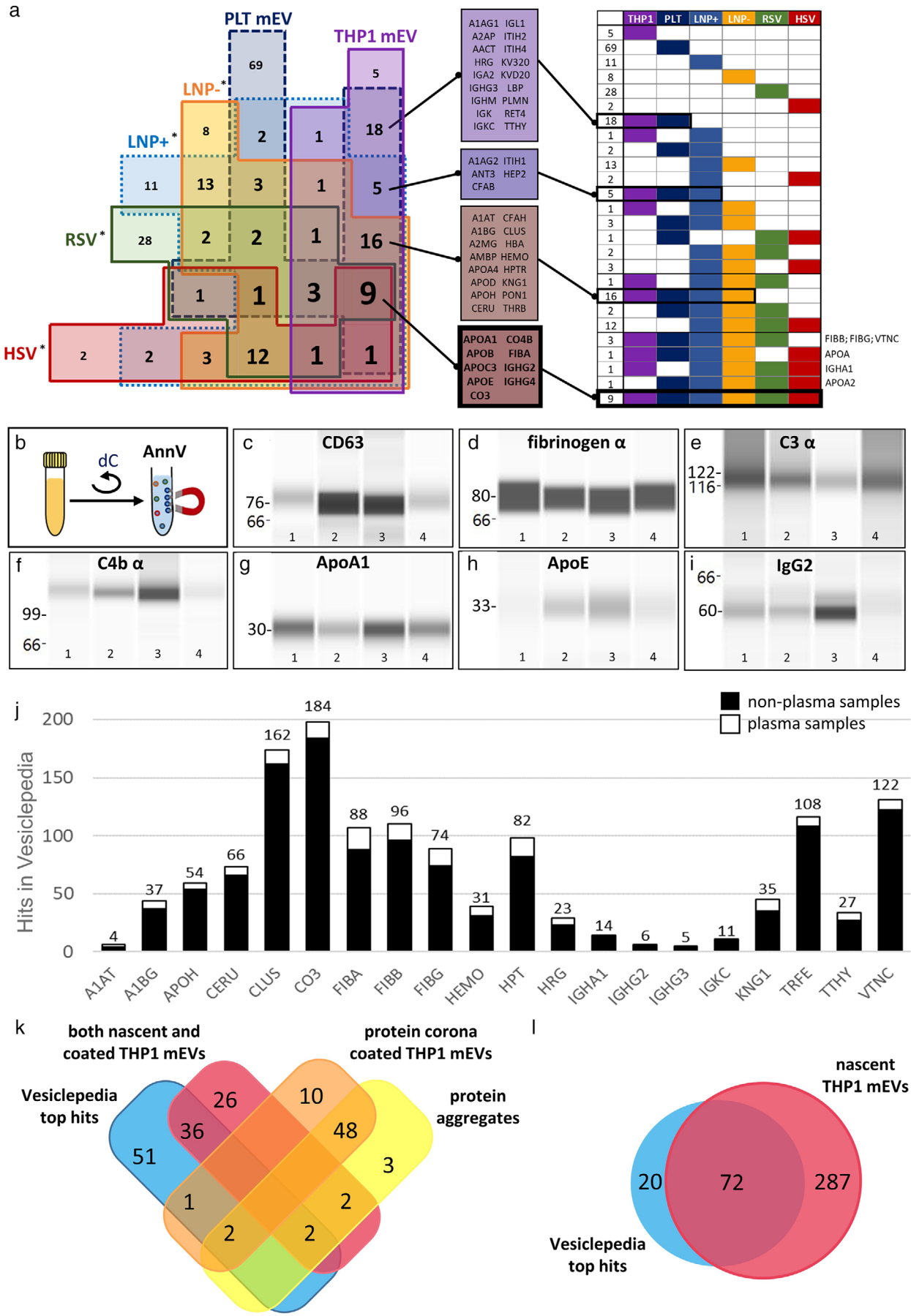
a
PLT mEV
THP1 mEV
LNP-*
LNP+*
RSV*
HSV*
69
5
8
2
1
18
11
13
3
1
5
28
2
2
1
16
1
1
3
9
2
2
3
12
1
1
A1AG1 IGL1
A2AP ITIH2
AACT ITIH4
HRG KV320
IGA2 KVD20
IGHG3 LBP
IGHM PLMN
IGK RET4
IGKC TTHY
A1AG2 ITIH1
ANT3 HEP2
CFAB
A1AT CFAH
A1BG CLUS
A2MG HBA
AMBP HEMO
APOA4 HPTR
APOD KNG1
APOH PON1
CERU THRB
APOA1 CO4B
APOB FIBA
APOC3 IGHG2
APOE IGHG4
CO3
THP1 PLT LNP+ LNP- RSV HSV
5
69
11
8
28
2
18
1
2
13
2
5
1
3
1
2
3
1
16
2
12
3
1
1
1
9
FIBB; FIBG; VTNC
APOA
IGHA1
APOA2
b
dC
AnnV
c
CD63
76-
66-
1 2 3 4
d
fibrinogen α
80-
66-
1 2 3 4
e
C3 α
122-
116-
1 2 3 4
f
C4b α
99-
66-
1 2 3 4
g
ApoA1
30-
1 2 3 4
h
ApoE
33-
1 2 3 4
i
IgG2
66-
60-
1 2 3 4
j
non-plasma samples
plasma samples
Hits in Vesiclepedia
200
150
100
50
0
4
37
54
66
162
184
88
96
74
31
82
23
14
6
5
11
35
108
27
122
A1AT
A1BG
APOH
CERU
CLUS
CO3
FIBA
FIBB
FIBG
HEMO
HPT
HRG
IGHA1
IGHG2
IGHG3
IGKC
KNG1
TRFE
TTHY
VTNC
k
both nascent and coated THP1 mEVs
protein corona coated THP1 mEVs
Vesiclepedia top hits
protein aggregates
26
10
36
48
51
3
1
2
2
2
l
nascent THP1 mEVs
20
72
287
Vesiclepedia top hits

the 180 putative THP1 mEV membrane proteins with the 61 corona proteins (detected in dC samples as described above) with the STRING database and web resource ((Szklarczyk *et al.*, 2019), https://string-db.org). Importantly, there is a limitation that STRING does not include human leukocyte antigen (HLA) and immunoglobulin molecules in the analysis. We considered only high confidence (score ≥ 0.700) interactions including physical and functional associations in the investigation. The predicted protein-protein interactions are represented in Figure 7a. The tabulated list of interactions (edges) is available in Table S13. Proteins not participating in interactions are not shown. As shown in the figure, there are multiple interactions both among corona proteins, and between the corona proteins and the mEV membrane proteins. There were only thirteen corona proteins that interacted with other corona proteins but not with membrane proteins. Interestingly, two of the nine 'shared corona proteins' were also identified among these proteins.

FIGURE 3 Comparison of viral, nanoparticle- and mEV-associated protein coronas formed in human plasma samples (a): The proteomic data of Ezzat *et al.* ((Ezzat *et al.*, 2019), marked with asterisks) on herpes simplex virus (HSV) and respiratory syncytial virus (RSV) as well as on positively (NP+) and negatively charged (NP-) artificial nanoparticles were re-analysed using a similar approach that we applied to identify EV corona proteins. The obtained protein lists were compared with proteins detected in ≥ 30% of the coated THP1 and platelet mEV samples (re-isolated by differential centrifugation (dC)). On the bottom right, next to the chart, we indicated those proteins that were missing from only one dataset. (b): Schematic illustration of the Annexin V-based affinity capture of blood plasma EV isolation from healthy samples ($n = 4$; individual samples are marked as 1–4 on each gel line) for Capillary Western (Wes) analysis. (c): CD63, (d): α chain of fibrinogen, (e): α chain of complement C3, (f): α chain of complement C4b, (g): ApoA1, (h): ApoE, (i): immunoglobulin G2. Molecular weights are indicated (kDa). (j): The 20 proteins that we detected in ≥ 90% of our plasma-coated mEV samples (re-isolated by dC) were searched in Vesiclepedia (Kalra *et al.*, 2012). The hits in the database are shown in the diagram. Empty portions of the columns correspond to blood plasma EV-associated protein entries, while the filled portions indicate protein entries of non-blood plasma derived EVs. (k): The Venn diagram shows the overlaps in Vesiclepedia top EV protein hits (top 92 proteins) with proteins shared by both nascent and coated THP1 mEVs, as well as with the corona proteins and with the pellets of EV-depleted blood plasma samples (corresponding to protein aggregates). All samples were prepared with dC. (l): Shared proteins in Vesiclepedia top hits (92 proteins) and nascent THP1 mEV samples.

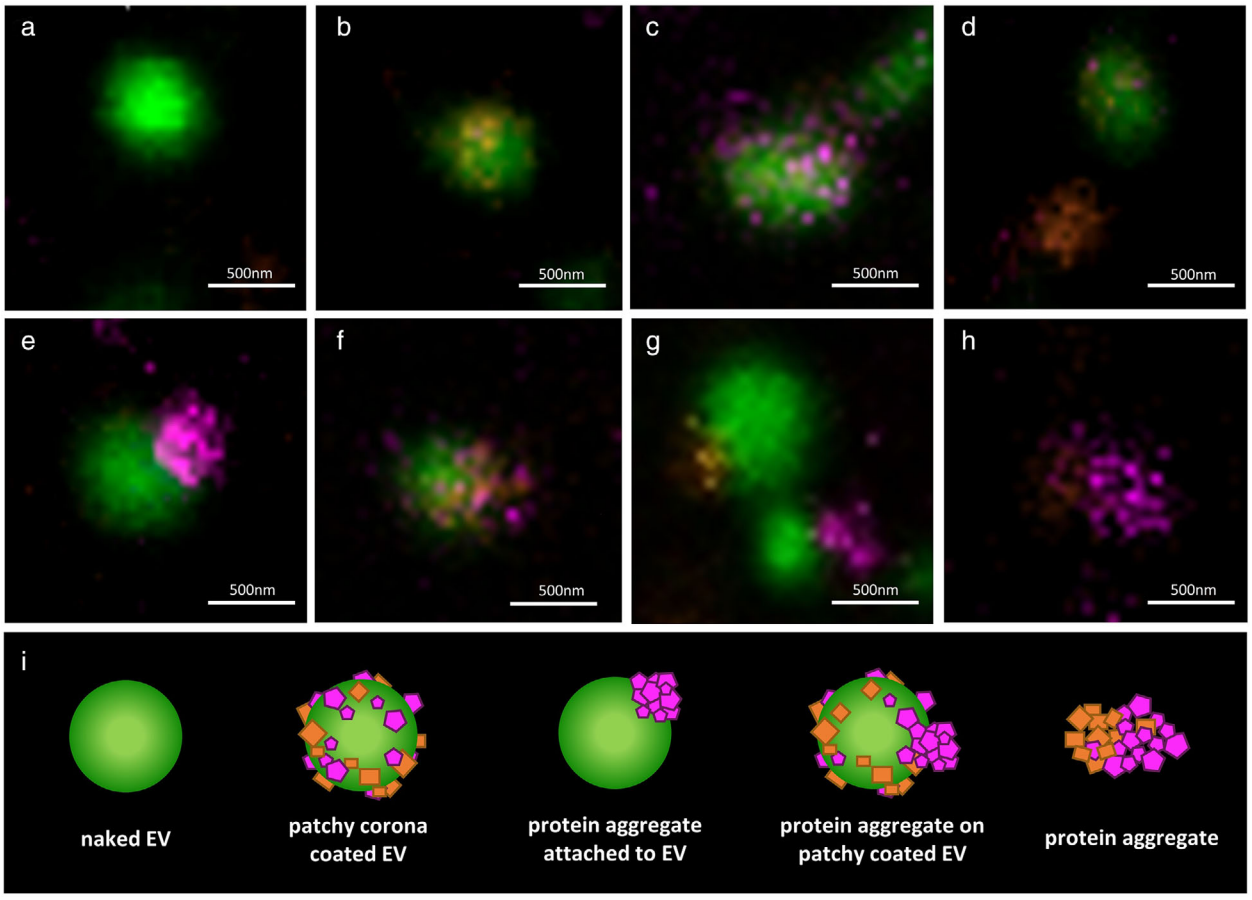

FIGURE 4 Confocal microscopy of EV-depleted blood plasma (EVDP)-coated mEVs. DiO-stained THP1 cell-derived nascent mEVs were incubated with healthy EVDP, washed twice and were immuno-stained with anti-fibrinogen α chain and anti-complement C3 antibodies, followed by Alexa647 and Alexa594 donkey anti-mouse and anti-rabbit antibodies, respectively. (a): mEV; (b): mEV with a patchy complement C3 corona; (c): mEVs with a patchy fibrinogen corona; (d): mEV with patchy fibrinogen and complement C3 deposition as well as a C3 aggregate; (e): mEV with associated fibrinogen aggregate; (f): mEV with patchy fibrinogen and complement C3 deposition as well as with a fibrinogen aggregate; (G): mEVs with associated fibrinogen and C3 aggregates; (h): aggregate of C3 and fibrinogen; (i): schematic illustration of the types of interactions of mEVs with proteins

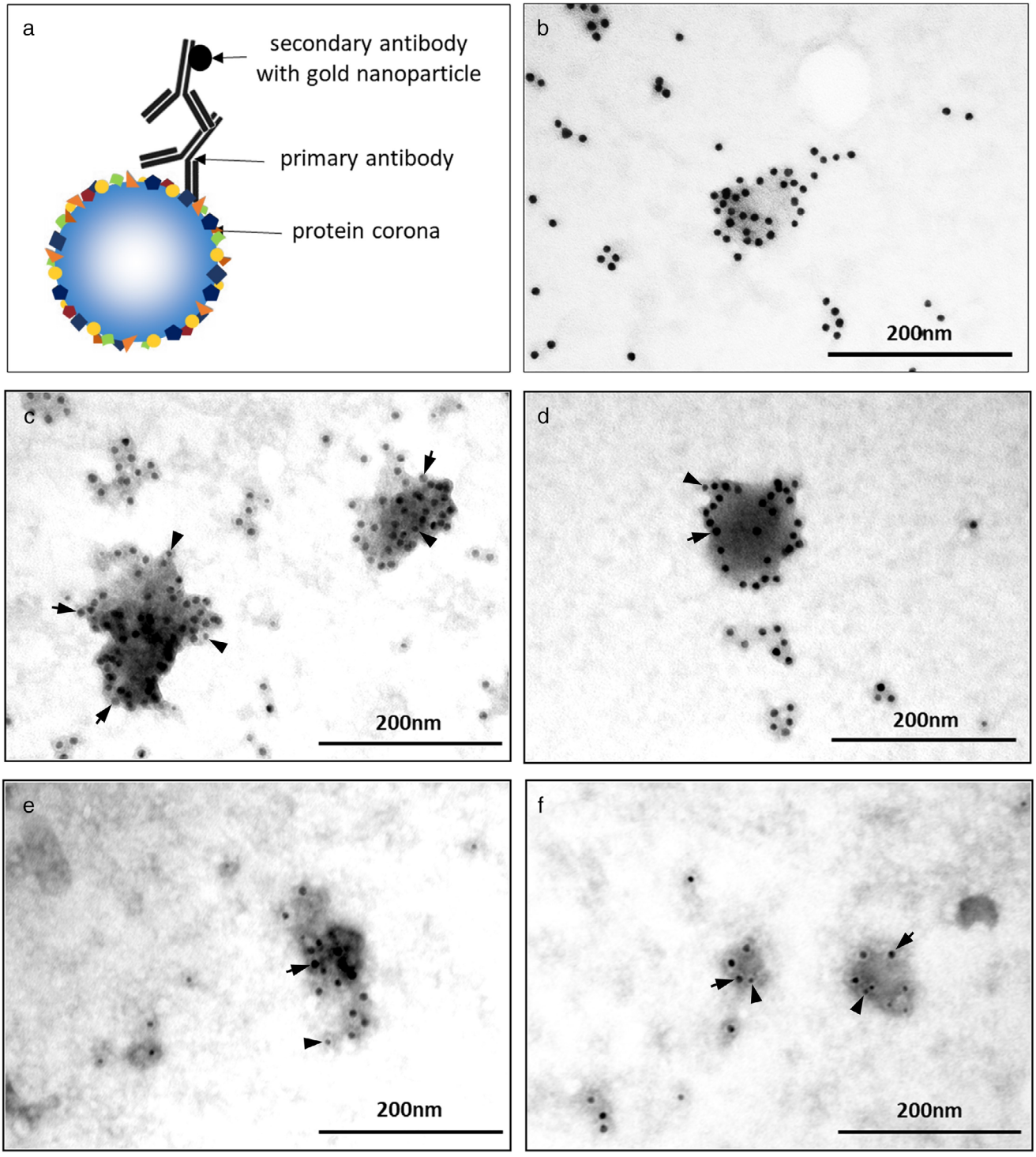

FIGURE 5 Detection of co-localization of corona proteins and mEV membrane proteins by immune electron microscopy. (a): Schematic illustration of the immunogold labelling. (b): THP-1 mEVs were re-isolated by differential centrifugation after incubation in EV-depleted blood plasma sample of a healthy person and were immuno-stained for the alpha chain of fibrinogen (10 nm gold particles), (c): for the alpha chain of fibrinogen and ApoA1 (10 and 5 nm gold particles, respectively), (d): for haptoglobin and CD63 (10 and 5 nm gold particles, respectively), (e): for complement C3 and CD63 (10 and 5 nm gold particles, respectively) and (f): for haptoglobin and ApoA1 (10 and 5 nm gold particles, respectively). Arrows indicate 10 nm, while arrowheads point to 5 nm gold particles

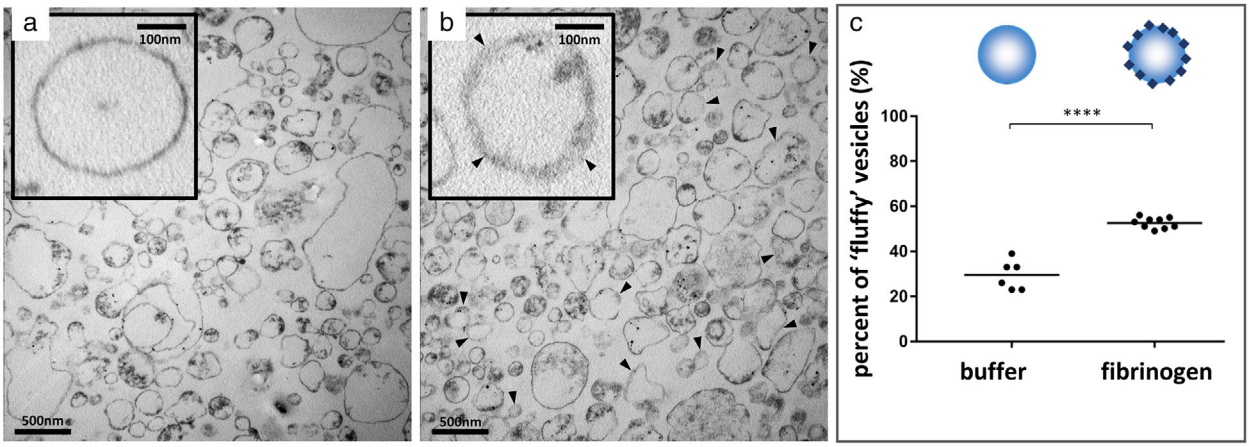

FIGURE 6 Imaging of fibrinogen-coated THP1 mEVs. Electron micrographs of mEVs either incubated in buffer (nascent mEVs, a), or in 1 mg/mL fibrinogen (coated mEVs, b). Arrowheads point to some mEVs with 'fluffy' (thickened) membrane. (c): Image analysis of nascent mEVs (six independent fields, $n = 596$ vesicles) and fibrinogen-coated EVs (eight independent fields, $n = 838$ vesicles) $P < 0.0001$, t-test.

To further characterize plasma protein association with mEVs, we co-incubated fluorochrome-labelled fibrinogen with nascent mEVs from Optiprep-purified platelets or from THP1 cells. As shown in Figure 7b–d, upon exposure to an increasing concentration of NaCl, the interaction of fibrinogen with the mEV surface could be disrupted. This was observed both in the case of mEVs of THP1 cells and of Optiprep-purified platelets (t-test $P < 0.05$ and $P < 0.01$, respectively).

3.4 | A number of plasma proteins detectable in the protein corona of mEVs can also be found in protein aggregates

To rule out the possibility that centrifugation and/or storage could cause protein aggregation in our samples, EVDPs as controls were also subjected to centrifugation and washing steps without the addition of THP1- or platelet-derived nascent mEVs (Figure 8). We analysed by MS the washed 'mock pellets' obtained (i) upon 12,500 g centrifugation of EVDPs (dC) as well as upon pelleting fractions in which mEVs are normally eluted, (ii) from DGUC, and (iii) from SEC (from the same HS EVDP samples, $n = 3$). Interestingly, with all EV separation methods, a high number of proteins were identified in the mock pellets. Out of them, 17 were common among all three methods (Figure 8a). The proteins identified in EVDP dC pellets ($n = 55$) are represented as a word cloud in Figure 8b. The tabulated list of proteins represented in Figure 8a-b are available in Table S14. Colour coding follows the coloured Venn diagram sections in panel A. In Table S15, we also compared the proteins of EVDP dC samples ($n = 22$) with the proteins of the mock pellets of the 3 HS samples that we analysed in Figure 8a–c. Importantly, most proteins (47/56 proteins detected in ≥ 30% of all 22 samples) were also present in the protein list obtained from the smaller sample set. In addition, in Table S16. we compared the mock pellets acquired with 12,500 g and with 20,000 g pelleting (HS, $n = 3$), where a similarly high overlap was detected. Figure 8c shows an unexpected overlap between the protein composition of protein aggregates and the protein corona. Importantly, these overlaps were found after dC/DGUC/SEC separation of the same three HS samples (coated THP1 mEVs and protein aggregates). As shown in the figure, both DGUC and SEC isolation resulted in a smaller overlap of the corona with protein aggregates. The widespread presence of protein aggregates in EVDPs raised the question, whether these protein aggregates could confound the detection of mEVs and the mEV protein corona components. The dC 'mock pellet' (protein aggregates) was therefore characterized by TRPS. The mode of particle diameter was around 200 nm and the particles in this 'mock pellet' were resistant to 0.1% Triton X-100 (Figure 8d). In contrast, as shown in the insert, mEVs were lysed efficiently in the presence of this Triton X-100 concentration. Immune electron microscopy of the 'mock pellets' (protein aggregates) obtained by dC of EVDP samples, revealed the presence of non-vesicular structures, most likely protein aggregates (Figure 8e), and importantly, we could not identify CD63 co-localization with the proteins in these samples. Confocal microscopy revealed the presence of DiO negative protein aggregates in the EVDP-coated mEV preparation separated by dC (Figure 8f). Finally, to see if repeated centrifugation of the original EVDP samples would itself result in an additional protein aggregation, and also, to find out whether it was feasible to get rid of protein aggregates by pelleting, we performed serial centrifugation of the EVDP samples with six consecutive rounds. The supernatants were removed carefully and re-centrifuged, while, the pellets were washed once in EV buffer before analysing their protein and lipid contents. While nascent THP1 mEVs had comparable amounts of proteins and lipids, only proteins were detectable in serially centrifuged 'mock pellets' (Figure 8g). These results suggested that the 'mock pellets' contained protein aggregates rather than EVs and that eliminating protein aggregates by serial centrifugation was not feasible.

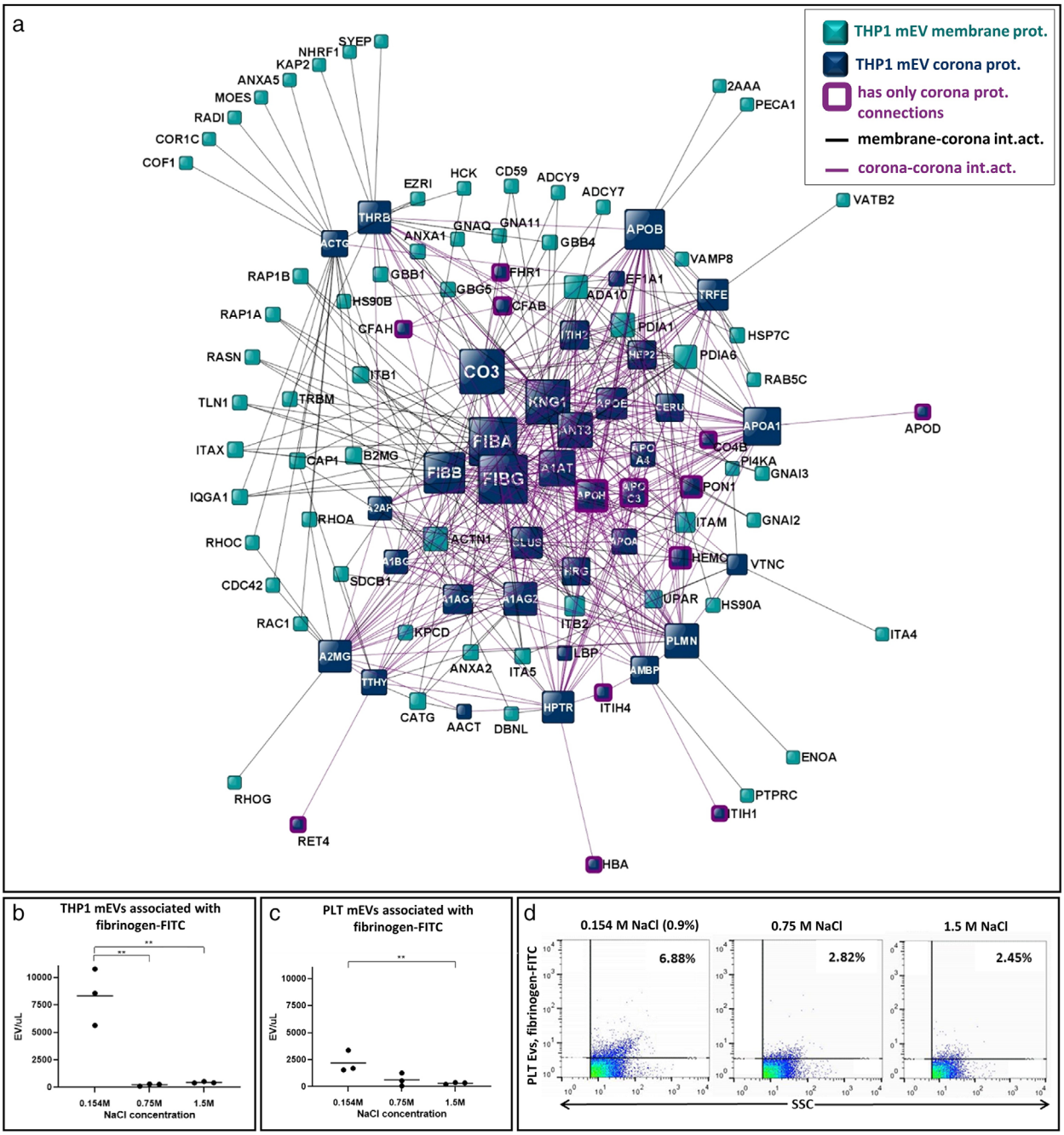

FIGURE 7 Interactions among corona proteins of mEVs and of corona proteins with the mEV surface. (a): Representation of protein-protein interactions identified with a high confidence (interaction score ≥ 0.700) with the STRING database and web resource ((Szklarczyk *et al.*, 2019), https://string-db.org). Interactions between the nascent THP1 mEV membrane proteins (with predicted membrane localisation according to the UniProt database (Bateman *et al.*, 2021)) and corona proteins are shown. Furthermore, interactions among the corona proteins are also indicated in purple colour. Out of the 107 network nodes, 61 represent membrane proteins while 46 represent corona proteins. Out of 515 edges, 203 show corona protein interactions with membrane proteins and 312 reflect interactions among corona proteins. We found 13 corona proteins (displayed with a purple node frame) to interact with other protein corona proteins only. Non-interacting proteins are not shown. All interaction sources (including physical and functional associations based on text mining, experiments, databases, co-expression, neighbourhood, gene fusion and co-occurrence) were considered in the analysis. Graph centrality measures were set based on the number of connected edges to each node. (b) and (c) show the association of fibrinogen-FITC with nascent THP1 and platelet mEVs, respectively. EV binding of the fluorescently labelled fibrinogen decreased significantly upon exposure of the samples to high concentration salt solutions. (*$P < 0.05$; **$P < 0.01$; t-test). (d): Representative flow cytometry dot plots show the fibrinogen-FITC binding to platelet mEVs.

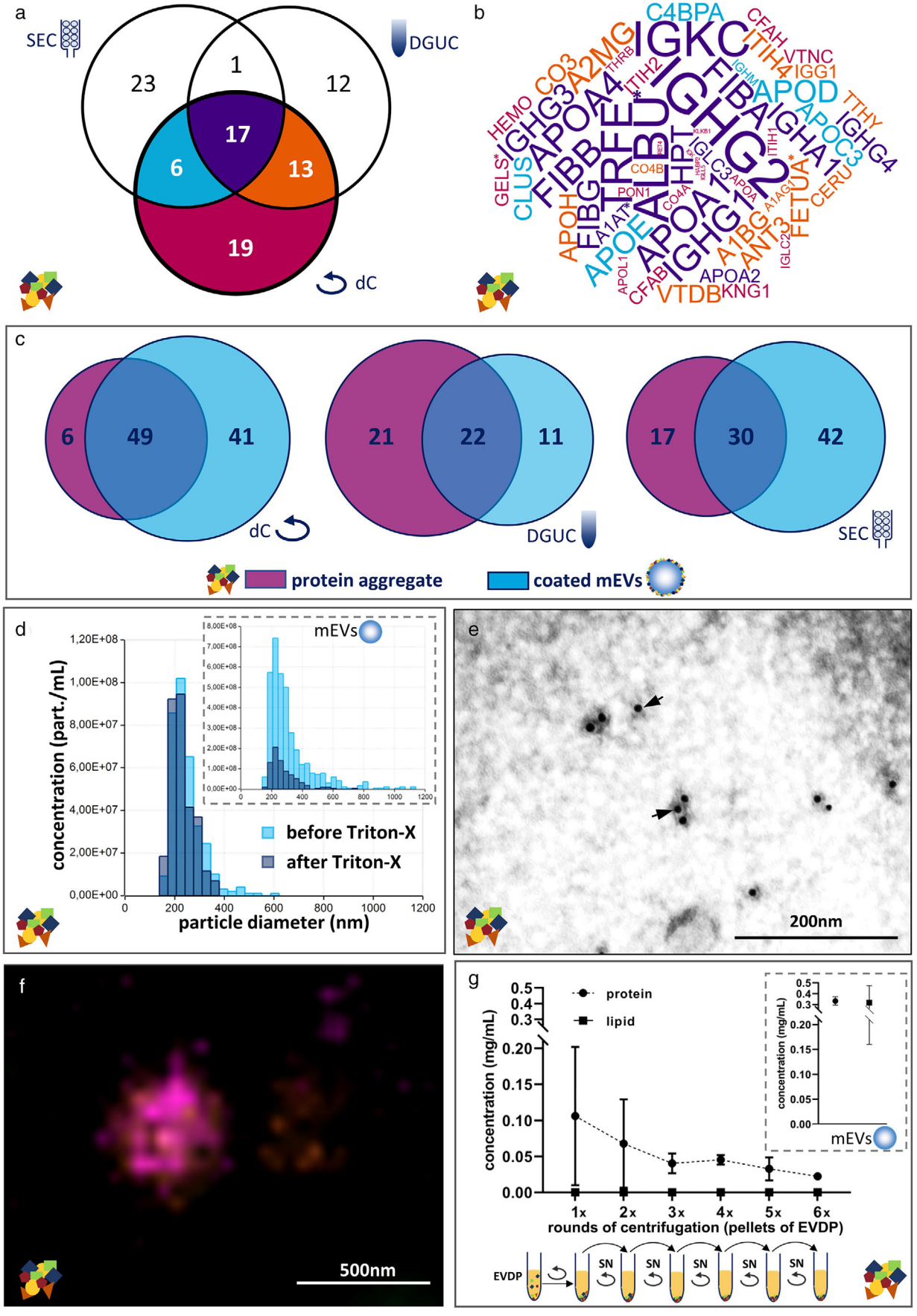
a
SEC
DGUC
23
1
12
17
6
13
19
dC
b
C4BPA
IGKC
CFAH
ITIH4
VTNC
IGG1
APOD
IGHG4
CO3
A2MG
THRB
ITIH2
IGHM
HEMO
APOA4
FIBB
FIBA
IGHA1
APOC3
CERU
GELS*
IGHG3
CLUS
APOH
FIBG
TRFE
ALB
HPT
IGL
KLKB1
ITIH1
C3
APOA
CO4B
PON1
CO4A
A1AT*
A1AG1*
FETUA
APOE
APOA1
IGHG1
A1BG
ANT3
IGLC2
APOL1
CFAB
APOA2
VTDB
KNG1
c
6
49
41
dC
21
22
11
DGUC
17
30
42
SEC
protein aggregate
coated mEVs
d
mEVs
concentration (part./mL)
particle diameter (nm)
before Triton-X
after Triton-X
e
200nm
f
500nm
g
protein
lipid
concentration (mg/mL)
rounds of centrifugation (pellets of EVDP)
mEVs
EVDP
SN

3.5 | Effects of nascent and coated THP1 mEVs as well as protein aggregates on monocyte-derived human dendritic cells (moDCs)

Monocyte-derived human dendritic cells were exposed to THP1 mEVs (re-isolated by dC) with/without pre-incubation in healthy or RA EVDP samples. The effects of these mEVs were compared to those of the protein aggregates (mock pellets of EVDP samples) isolated from identical aliquots of EVDP samples (Figure 9a). As shown in Figure 9b, coated EVs induced significant TNF-α production by moDCs in contrast to the nascent ones (healthy and RA EVDP-incubated mEVs, $P < 0.05$ and $P < 0.001$; respectively; Kruskal-Wallis analysis with Dunn's post-test). Furthermore, there was a significant difference between the effect of RA-coated mEVs and protein aggregates derived from the same EVDP samples ($P < 0.01$; Kruskal-Wallis analysis with Dunn's post-test). The production of IL-6 was also significantly higher in the presence of RA-coated mEVs as compared to the RA plasma protein aggregates ($P < 0.05$; Kruskal-Wallis analysis with Dunn's post-test) (Figure 9c). The frequency of CD83 positive mature moDCs as well as the HLA-DR mean fluorescence intensity showed a significant elevation upon exposure to mEVs alone, or incubated either in healthy or RA plasma samples compared to the buffer control (unstimulated) and to protein aggregates ($P < 0.05$, $P < 0.01$ or $P < 0.001$ as indicated in the figure; One-way ANOVA with Tukey's multiple comparisons test) (Figure 9d,e). Similarly, we saw an increased frequency of CD86 positive moDCs upon exposure to RA EVDP coated mEVs as compared to the buffer control (unstimulated) and to RA EVDP-derived protein aggregates as well as upon exposure to HS EVDP coated mEVs as compared to HS protein aggregates ($P < 0.05$ or $P < 0.01$ as indicated in the figure; One-way ANOVA with Tukey's multiple comparisons test) (Figure 9f).

To clarify if the protein corona affected association of EVs with cells, we exposed peripheral blood cells to nascent and coated THP1 mEVs. mEVs of DiO-stained THP1 cells were separated, coated with HS EVDP or kept in EV buffer and were re-isolated by dC. Identical number of fluorescent mEVs were added to peripheral blood cells and the association of the mEVs with cells was measured by flow cytometry after 45 min. Cells in the lymphocyte, monocyte and neutrophil gates showed an association with both the membrane-labelled nascent and coated THP1 mEVs; however, only lymphocytes showed a significantly increased association with coated mEVs as compared to the nascent ones (one-way ANOVA with Tukey's post-test, $P < 0.05$) (Figure S7).

4 | DISCUSSION

Extracellular vesicles have received a lot of attention in the past few years and are increasingly recognized as cell-derived subcellular structures released to the extracellular space. EVs are commonly separated from conditioned media and biological fluids, and more recently even from tissues (Crescitelli *et al*., 2020; Jang *et al*., 2019; Vella *et al*., 2017). The separation approaches range from precipitation techniques, dC, SEC and DGUC, affinity capture methods, microfluidics, flow field flow fractionation, etc. However, no matter what EV separation method is applied, yet there is no technique that would yield pure EV preparations (Théry *et al.,* 2018). In particular, in blood plasma-derived EV preparations, which hold enormous potential as biomarkers in liquid biopsies, protein contamination from the protein-rich matrix is a major problem. Both the plasma membrane of cells and the EVs which are shed from the plasma membrane are in continuous contact with the surrounding interstitial fluid or blood plasma. Thus, not surprisingly, the surface of EVs is a stage of diverse molecular interactions (Buzás *et al*., 2018).

A special interaction of blood plasma proteins with the surface of artificial nanoparticles has long been known as 'protein corona' formation (Cedervall *et al*., 2007). Artificial nanoparticles have been intensively studied in vivo for drug delivery. The formation of a protein corona on the surface of these therapeutic particles has been shown to have a major influence on the bioavailability and bio-distribution of these structures (as reviewed in (Xiao & Gao, 2018)). Recently, a similar protein corona formation has also been demonstrated around virus particles (Ezzat *et al*., 2019) and importantly, viruses are known to show

FIGURE 8 Characterization of plasma protein aggregates. (a): The Venn diagram indicates the number of proteins identified by mass spectrometry in the washed pellets of healthy EV-depleted blood plasma (EVDP) samples ($n = 3$) corresponding to protein aggregates. Identical EVDP samples were processed by three different methods (differential centrifugation (dC), DGUC and SEC, indicated with symbols). (b): Word cloud illustration of the coloured section of panel A. The different colours mark the proteins detected either only with dC, or also with SEC or DGUC or with all of these methods. The font size correlates with the percentage of detection of a given protein among the samples. Asterisks indicate those proteins that were also identified in the nascent THP1 mEV samples and therefore were not included in the primary list of corona proteins. (c): Overlaps of the corona proteins with protein aggregates separated from the same three healthy EVDP samples with three different methods. (d): Representative TRPS histogram of a twice-washed EVDP pellet separated by dC (measured before and after 0.1% Triton-X lysis). For comparison, the insert shows the effect of the detergent lysis on a nascent THP1 mEVs. (e): Immunogold-stained electron micrograph of a twice-washed 12,500 g healthy EVDP pellet. The sample was stained for haptoglobin and CD63 (10 and 5 nm gold particles, respectively). Arrows indicate 10 nm gold particles (CD63 was not identified with 5 nm gold particles in the sample). (f): Confocal microscopic image of a mixed fibrinogen and complement C3 aggregate in a EVDP-coated mEV preparation (immuno-stained with anti-fibrinogen α chain and anti-complement C3 antibodies and Alexa 647 and Alexa 594 donkey anti-mouse and anti-rabbit antibodies respectively) (g): Healthy EVDP samples ($n = 3$) were subjected to serial centrifugation at 12,500 g for 40 min. Protein and lipid concentrations of the washed pellets were determined after each run. While the lipid concentration was under the detection limit throughout the analysis, proteins were detectable in the pellet even after the 6^{th} round of centrifugation. For comparison, the insert shows protein and lipid concentrations of nascent mEV samples ($n = 3$)

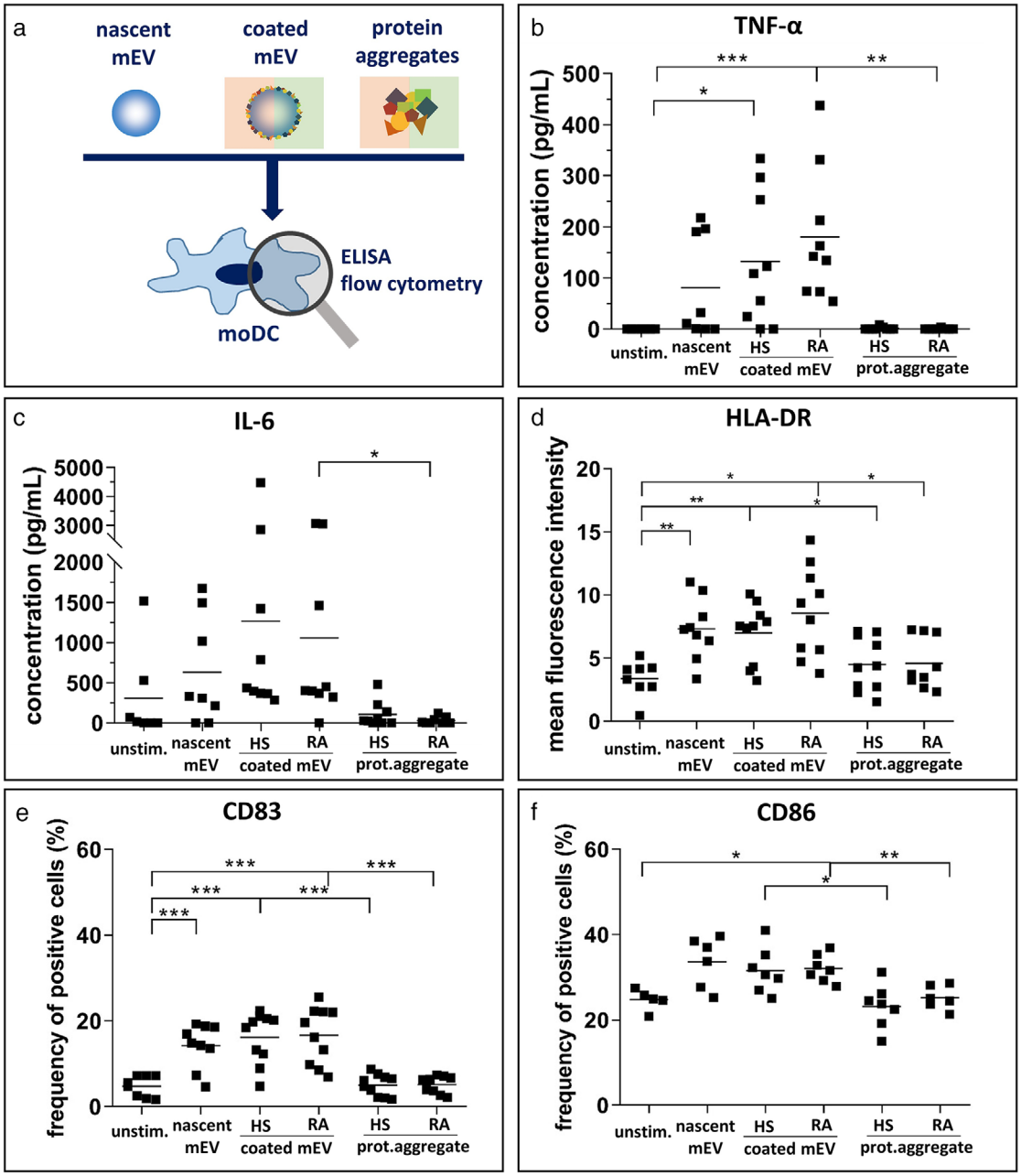

FIGURE 9 The effects of corona-coated mEVs on human monocyte-derived dendritic cells. Human monocyte-derived dendritic cells (moDCs) were differentiated *ex vivo* in the presence of IL-4 and GM-CSF for 5 days. MoDCs were then exposed to nascent- or plasma protein-coated vesicles or to pellets of EVDP samples (protein aggregates) separated with differential centrifugation. The production of TNF-α and IL-6 was determined by ELISA. The frequency of CD83 and CD86 positive cells as well as the mean fluorescence intensity of HLA-DR positive cells was assessed by flow cytometry. HS: healthy subjects; RA: patients with rheumatoid arthritis; unstim.: unstimulated, cells treated with EV buffer; prot. aggregate: protein aggregate. Kruskal-Wallis analysis with Dunn's post-test (TNF-α and IL-6), One-way ANOVA with Tukey's multiple comparisons test (CD83, CD86 and HLA-DR), *: $P < 0.05$, **: $P < 0.01$, ***: $P < 0.001$

striking similarity with EVs (Nolte-'t Hoen *et al.,* 2016). Therefore, it was tempting to hypothesize that similarly to artificial nanoparticles and viruses, a protein corona is formed also around EVs. For artificial nanoparticles, the determination of corona proteins proved to be relatively simple because the components of these nanoparticles do not interfere with determination of corona proteins. Even in the case of viruses, the known composition of certain virions facilitates identification of corona proteins derived from the mammalian host. The difficulty of EV corona analysis is that both the corona and the EV proteins are derived from the same host organism. In addition, EVs are heterogeneous, therefore identifying which molecules belong to the protein corona and which are components of EVs proves to be challenging. Although the protein composition of separated plasma EVs has been already compared with published proteomic datasets of both EV preparations and artificial nanoparticle coronas,

and based on this, the existence of a protein corona around EVs has already been proposed (Palviainen *et al.*, 2020), no direct experimental evidence has been provided so far about the formation of an EV protein corona.

Here we used the approach to harvest nascent EVs from serum-free conditioned medium of THP1 cells and Optiprep-purified platelets and to incubate these vesicles in EVDP samples. Our MS results obtained after dC, SEC or DGUC provided evidence for the presence of EV-associated proteins. The corona was also detectable by Wes, confocal microscopy, transmission and immune EM and was also reflected by an increased floatation density of 'coated EVs'. Some of the corona proteins could be dissociated from the EV surface in the presence of high salt solution suggesting electrostatic interactions in the corona formation.

We next compared published datasets of protein coronas formed in human blood plasma around viruses (such as HSV and RSV) and lipid nanoparticles (of the size of approx. 200 nm) with our THP1 and platelet EV data. One of the most exciting results of this study was that we found nine proteins that were present in all six datasets (THP1 and platelet mEVs, HSV, RSV, positively and negatively charged lipid nanoparticles). Furthermore, these nine proteins were also detected in several other previous studies on artificial nanoparticles (Brückner *et al.*, 2020; Di Santo *et al.*, 2020; Digiacomo *et al.*, 2020; Giulimondi *et al.*, 2019; Papafilippou *et al.*, 2020; Weber *et al.*, 2018). Given that the analysed datasets resulted from somewhat different preparative and analytical approaches, the finding that nine proteins were shared by all protein coronas was even more unexpected. Surprisingly, these nine shared proteins were known opsonins such as apolipoproteins, complement and clotting factors and immunoglobulins. Despite the abundance of opsonins in the protein corona, we could not show a major impact of the corona on the association of mEVs with phagocytic cells such as neutrophils and monocytes. This may argue against that the primary role of the corona is to facilitate EV uptake by cells.

Of note, Palviainen *et al.* (Palviainen *et al.*, 2020) compared proteins of their ultracentrifuged PFP pellets with those reported in (i) EV-related, and (ii) synthetic nanoparticle-related published proteomic datasets. Based on the first comparison, the authors proposed 34 EV surface-associated proteins out of which we found 5/9 to be identical with our universal protein corona (these matched proteins included ApoA1, ApoE, complement factor 3, complement factor 4B and fibrinogen α-chain). Upon the second type of comparison, the authors suggested 46 corona proteins from among which again five were identical with our nine universal corona proteins including ApoC3, ApoE, complement factor 3, fibrinogen α-chain, and immunoglobulin heavy constant γ4 (IgG4). Thus, the findings of Palviainen *et al.* and our current work synergistically prove that EV associated proteins are not just 'contaminants' of EV preparations.

It may seem unexpected that albumin is not present in our list of nine corona proteins. The reason is that in our analysis, albumin was detected in nascent EV preparations of THP1 cells as well. We found that THP1 cells indeed expressed albumin (Figure S8). The question is further complicated by the published observations that certain extracellular proteins such as complement C3 and fibronectin are secreted on the surface of nascent small EVs (Carrillo-Conde *et al.*, 2012; Papp *et al.*, 2008; Sung *et al.*, 2015). In addition, our data also point to the fact that the EV releasing cells themselves carry extracellular proteins in association with their plasma membrane (Figure S9). Importantly, we have recently demonstrated the widespread presence of bovine proteins in lysates of human cell lines (Sugár *et al.*, 2020). We hypothesized that this was most probably due to internalized proteins of the foetal calf serum containing medium. Based on our data, here we propose that corona formation might not only take place *in vivo* in biological fluids, but also in foetal bovine serum supplemented tissue culture media of in vitro experiments (irrespective whether using normal or EV-depleted FBS). In our analysis of a plasma protein-coated EV sample, 153 proteins were of human origin, two proteins were bovine, and in the case of 26 proteins, the bovine or human origin could not be determined based on the tryptic fragments (Dataset S2). The high number of plasma proteins in non-plasma derived EV proteomic datasets of Vesiclepedia also supports the concept that EV-associated proteins may at least partially originate from FBS.

In the case of artificial nanoparticles, the formation of a personalised protein corona (characteristic for a given individual) has been described (Corbo *et al.*, 2017). Based on this observation, here we were also interested whether EV corona formation in plasma samples of healthy subjects or patients with RA showed any remarkable disease-related or individual differences. The most common corona proteins were shared by all corona-coated EVs irrespective of the origin of the blood plasma. However, we could demonstrate the enrichment of certain proteins in association with EVs incubated in the plasma of patients with RA. These RA-related EV corona proteins were present in the more individual protein coronas as they were found mostly in $< 50\%$ of all samples. Our WES analysis also revealed individual corona protein patterns on plasma derived mEVs. A limitation of our study was that there was a significant age difference between the healthy and RA EVDP donors which could have also impacted our results.

DCs are the most sensitive sensors of the innate immune system to detect molecular changes in the extracellular microenvironment (including alterations in DAMPs). Therefore, we tested moDCs for their ability to respond to healthy and inflammatory disease (RA)-related protein coronas on EVs. Surprisingly, the RA-related EV coat did not induce a different response in moDCs as compared to the healthy plasma-related corona. However, we cannot exclude the possibility that more active RA patient-derived coronas could have induced a more prominent effect. On the other hand, EVs with both healthy and RA coronas efficiently induced both TNF-α secretion of moDCs and moDC maturation (reflected by CD83, CD86 and HLA-DR expression) in contrast to nascent mEVs or protein aggregates. Of note, the elevated TNF-α production by moDCs exposed to corona-coated mEVs (irrespective of the origin of the protein coat) may suggest a tonic pro-inflammatory role of these mEVs. This effect may

maintain T cell responsiveness, and under conditions with enhanced EV release (e.g., in inflammation), it may contribute to a deviation from the immune equilibrium.

After many groups have observed the presence of plasma proteins as 'contaminants' in their EV samples, here we provide evidence for a protein corona formation around EVs. This corona formation may occur universally in biofluids and components of the corona might be characteristic for the surrounding matrix. The mechanism behind this corona formation presumably involve protein aggregation and electrostatic interactions as well. However, beside this non-specific passive adsorption of proteins on the surface of EVs, specific, receptor-ligand interactions may also play a role in corona protein-EV surface association. Based on our observations, we may consider the 'contaminating' corona proteins as inevitable external molecular components of EVs.

Although in the present study we only analysed protein coronas of mEVs, data published by others strongly suggest similar protein interactions with the surface of small EVs (sEVs) as well. As an example, the group of C. Théry demonstrated the association of several serum and ECM proteins (e.g., albumin, complement proteins, prothrombin and fibronectin) with what they called 'dense sEVs', EVs with enhanced floatation density (Kowal *et al*., 2016). This is similar to our results showing that 'coated mEVs' had a higher floatation density as compared to 'nascent' ones. Another published indication of the association of bovine plasma proteins with sEVs has been published recently upon affinity-based EV isolation (Nakai *et a*l., 2016).

An unexpected finding of our current study was the abundance of protein aggregates in pellets after centrifugation of EVDP at medium speed (12,500 g 40 min). This protein aggregate formation was observed in EVDP samples even after six consecutive rounds of 12,500 g centrifugation. This was in spite of that the EV-depletion of plasma samples included a serial filtration of PFPs through 5 μm and 0.8 μm filters followed by a 40 min 20,000 g and an overnight 100,000 g centrifugation. The finding that the EVDP was an almost unlimited source of protein aggregates even at the low speed commonly used to separate mEVs, points to the importance of careful characterization of blood plasma-derived EVs. Our EVDP samples were stored frozen (-80°C) for up to 6 months prior to our experiments, and freezing-thawing may undoubtedly induce protein aggregation (Mahler *et al.,* 2009). Furthermore, centrifugation even at low speed may cause agitation or shear stress also known to induce protein aggregation (Mahler *et al*., 2009). Given that storage of biological samples in a frozen form and centrifugation at least at low speed are both common in EV studies, our results point to severe limitations of protein or particle number-based EV standardization. Despite these days, there is an increasing awareness in the scientific community that lipoproteins may obscure particle number-based EV standardization (Sódar *et al*., 2016), less attention has been paid lately to protein aggregation in EV containing samples. Several years ago, we were the first to drive the attention of the field to the shared biophysical parameters of EVs and protein aggregates, and we introduced differential detergent lysis to distinguish mEVs and protein complexes (György *et al*., 2011). Later, we have also shown that thiol-based EV detection with maleimide should always be combined with immunostaining for EV membrane proteins because of the presence and interference with thiol containing protein aggregates (Szabó-Taylor *et al*., 2017). Furthermore, we also found that upon mixing nascent EVs with LDL particles, almost instantaneously an LDL corona was formed around EVs (Sódar *et al.,* 2016). Finally, we reported the association of DNA (predominantly mitochondrial DNA) with the surface of sEVs under genotoxic stress conditions (Németh *et al*., 2017). All these observations suggest that a biomolecular corona rather than just a protein corona formation occurs once nascent EVs get in contact with the extracellular molecules. This biomolecular corona formation may be similar to what has been observed in the case of artificial nanoparticles where authors also found corona components other than proteins (such as lipids, complete HDL particles, fatty acids and small organic compounds) (Caracciolo, 2018; Gunnarsson *et al*., 2018; Hellstrand *et al*., 2009; Kapralov *et al*., 2012; La Barbera *et al.,* 2020; Lee *et al*., 2018; Martel *et al.,* 2016; Müller *et al*., 2018; Pink *et al*., 2018; Raesch *et al*., 2015).

In our current study, DiO-stained EVs were shown to carry both a diffuse (patchy) protein corona which was in line with prior expectations. Interestingly, we found large protein aggregates attached to EVs as well. This finding provides a straightforward explanation for the detected high proteomic overlap between corona-coated EVs and protein aggregates. The immune EM detection of corona proteins co-localizing with CD63 around EVs provided further evidence to the association of a protein corona to EVs. Classes of plasma membrane proteins include two major categories namely integral and peripheral proteins. We propose that the EV surface associated proteins could be also considered as peripheral EV membrane proteins. However, it remains unclear whether these proteins form single or multiple layers around the vesicular membrane.

Furthermore, to fully understand the functional significance of the protein corona around EVs, several additional studies are required. The presence of the corona may influence vesicle mobility (Skliar *et al*., 2018) and diameter as well (Varga *et al.,* 2020). The most convincing data about the functional significance of EV surface-associated proteins come from a recent study (Willis *et al*., 2019). In this work, the authors found that EV-associated fibrinogen induced encephalitogenic CD8+ T cells in experimental autoimmune encephalomyelitis, a mouse model of multiple sclerosis. More recently, Busatto *et al.* have demonstrated that pro-metastatic vesicles establish distinct associations with LDL, and this interaction affects the uptake of EVs by monocytes (Busatto *et al*., 2020).

In conclusion, here we demonstrated that in biological fluids, a protein corona is formed spontaneously around the surface of EVs. Our results suggest a potential significance of protein aggregation in this process. A wide-ranging implication of our findings is that most of the artificial nanoparticle and virus protein corona studies also involved centrifugation steps. Our data also provide an explanation for the presence of blood plasma protein 'contamination' commonly found in EV preparations by most research groups.

ACKNOWLEDGEMENTS

This work was supported by the National Research, Development and Innovation Office NKFIH, Hungary under Grant number OTKA11958, OTKA120237, OTKA125337, OTKA K 131479, OTKA PD 121187, OTKA FK 131603, OTKA 131762, NVKP_16-1-2016-0017, Higher Education Institutional Excellence Program – Therapeutic development, ÚNKP-19-3-I-SE-45 and ÚNKP-20-5 – New National Excellence Program of the Ministry for Innovation and Technology; Ministry for National Economy of Hungary under Grant number VEKOP-2.3.2-16-2016-00002, VEKOP-2.3.3-15-2017-00016, EFOP-3.6.3-VEKOP-16-2017-00009: Az orvos-, egészségtudományi- és gyógyszerészképzés tudományos műhelyeinek fejlesztése;European Commission under Grant number H2020-MSCA-ITN-2017-722148 TRAIN EV; Hungarian Academy of Sciences under Grant János Bolyai Research Scholarship and "Momentum" research grant (LP2016-4/2016);European Research Council under Grant ERC-CoG 724994, and H2020-ITN-2018-813294-ENTRAIN. The project has also received funding from the EU's Horizon 2020 research and innovation program under grant agreement No. 739593

CONFLICT OF INTEREST

EIB is member of the Advisory Board of Sphere Gene Therapeutics Inc. (Boston, USA).

ORCID

Edit I. Buzás https://orcid.org/0000-0002-3744-206X

REFERENCES

Aatonen, M. T., Öhman, T., Nyman, T. A., Laitinen, S., Grönholm, M., & Siljander, P. R.M. (2014). Isolation and characterization of platelet-derived extracellular vesicles. *Journal of Extracellular Vesicles*, *3*, 24692. https://doi.org/10.3402/jev.v3.24692

Aletaha, D., Neogi, T., Silman, A J., Funovits, J., Felson, D T., Bingham, C O., Birnbaum, N S., Burmester, G R., Bykerk, V P., Cohen, M D., Combe, B., Costenbader, K H., Dougados, M., Emery, P., Ferraccioli, G., Hazes, J M. W., Hobbs, K., Huizinga, T W. J., Kavanaugh, A.…Hawker, G. (2010). Rheumatoid arthritis classification criteria: an American College of Rheumatology/European League Against Rheumatism collaborative initiative. *Arthritis and Rheumatism*, *62*(9), 2569–2581. https://doi.org/10.1002/art.27584

Aswad, H., Jalabert, A., & Rome, S. (2016). Depleting extracellular vesicles from fetal bovine serum alters proliferation and differentiation of skeletal muscle cells in vitro. *Bmc Biotechnology [Electronic Resource]*, *16*, 32–32. https://doi.org/10.1186/s12896-016-0262-0

Baranyai, T., Herczeg, K., & Onódi, Z. *et al.* (2015). Isolation of exosomes from blood plasma: Qualitative and quantitative comparison of ultracentrifugation and size exclusion chromatography methods. *PLoS One*, *10*(12), e0145686. https://doi.org/10.1371/journal.pone.0145686

Bateman, A., Martin, M. J., Orchard, S., Magrane, M., Agivetova, R., Ahmad, S., Alpi, E., Bowler-Barnett, E. H., Britto, R., Bursteinas, B., Bye-A-Jee, H., Coetzee, R., Cukura, A., Da Silva, A., Denny, P., Dogan, T., Ebenezer, T., Fan, J., Castro, L. G.…Teodoro, D. (2021).UniProt: The universal protein knowledgebase in 2021. *Nucleic Acids Research*, *49*(D1), D480–D489. https://doi.org/10.1093/nar/gkaa1100

Brückner, M., Simon, J., Jiang, S., Landfester, K., & Mailänder, V. (2020). Preparation of the protein corona: How washing shapes the proteome and influences cellular uptake of nanocarriers. *Acta Biomaterialia*, *114*, 333–342. https://doi.org/10.1016/j.actbio.2020.07.041

Busatto, S., Yang, Y., Walker, S. A., Davidovich, I., Lin, W. H., Lewis-Tuffin, L., Anastasiadis, P. Z., Sarkaria, J., Talmon, Y., Wurtz, G., & Wolfram, J. (2020). Brain metastases-derived extracellular vesicles induce binding and aggregation of low-density lipoprotein. *Journal Nanobiotechnology*, *18*(1), 162. https://doi.org/10.1186/s12951-020-00722-2

Buzas, E. I., György, B., Nagy, G., Falus, A., & Gay, S. (2014). Emerging role of extracellular vesicles in inflammatory diseases. *Nature Clinical Practice Rheumatology*, *10*(6), 356–364. https://doi.org/10.1038/nrrheum.2014.19

Buzás, E. I., Tóth, E. Á., Sódar, B. W., & Szabó-Taylor, K. É. (2018). Molecular interactions at the surface of extracellular vesicles. *Seminars in Immunopathology*, *40*(5), 453–464. https://doi.org/10.1007/s00281-018-0682-0

Caracciolo, G. (2018). Clinically approved liposomal nanomedicines: Lessons learned from the biomolecular corona. *Nanoscale*, *10*(9), 4167–4172. https://doi.org/10.1039/c7nr07450f

Carrillo-Conde, B. R., Ramer-Tait, A. E., Wannemuehler, M. J., & Narasimhan, B. (2012). Chemistry-dependent adsorption of serum proteins onto polyanhydride microparticles differentially influences dendritic cell uptake and activation. *Acta Biomaterialia*, *8*(10), 3618–3628. https://doi.org/10.1016/j.actbio.2012.06.001

Cedervall, T., Lynch, I., Lindman, S., Berggard, T., Thulin, E., Nilsson, H., Dawson, K. A., & Linse, S. (2007). Understanding the nanoparticle-protein corona using methods to quantify exchange rates and affinities of proteins for nanoparticles. *Proceedings of the National Academy of Sciences of the United States of America*, *104*(7), 2050–2055. https://doi.org/10.1073/pnas.0608582104

Corbo, C., Molinaro, R., Tabatabaei, M., Farokhzad, O. C., & Mahmoudi, M. (2017). Personalized protein corona on nanoparticles and its clinical implications [10.1039/C6BM00921B]. *Biomaterials Science*, *5*(3), 378–387. https://doi.org/10.1039/C6BM00921B

Crescitelli, R., Lässer, C., Jang, Su C., Cvjetkovic, A., Malmhäll, C., Karimi, N., Höög, J. L., Johansson, I., Fuchs, J., Thorsell, A., Gho, Y. S., Olofsson Bagge, R., & Lötvall, J. (2020). Subpopulations of extracellular vesicles from human metastatic melanoma tissue identified by quantitative proteomics after optimized isolation. *Journal of Extracellular Vesicles*, *9*(1), 1722433. https://doi.org/10.1080/20013078.2020.1722433

Cvjetkovic, A., Jang, Su C., Konečná, B., Höög, J. L., Sihlbom, C., Lässer, C., & Lötvall, J. (2016). Detailed analysis of protein topology of extracellular vesicles–evidence of unconventional membrane protein orientation. *Scientific Reports*, *6*(1), 36338. https://doi.org/10.1038/srep36338

Di Santo, R., Digiacomo, L., Quagliarini, E., Capriotti, A. L., Laganà, A., Zenezini Chiozzi, R., Caputo, D., Cascone, C., Coppola, R., Pozzi, D., & Caracciolo, G. (2020). Personalized graphene oxide-protein corona in the human plasma of pancreatic cancer patients. *Frontiers in Bioengineering and Biotechnology*, *8*, 491–491. https://doi.org/10.3389/fbioe.2020.00491

Digiacomo, L., Jafari-Khouzani, K., Palchetti, S., Pozzi, D., Capriotti, A. L., Laganà, A., Zenezini Chiozzi, R., Caputo, D., Cascone, C., Coppola, R., Flammia, G., Altomare, V., Grasso, A., Mahmoudi, M., & Caracciolo, G. (2020). A protein corona sensor array detects breast and prostate cancers [10.1039/D0NR03439H]. *Nanoscale*, *12*(32), 16697–16704. https://doi.org/10.1039/D0NR03439H

Eitan, E., Zhang, S., Witwer, K. W., & Mattson, M. P. (2015). Extracellular vesicle-depleted fetal bovine and human sera have reduced capacity to support cell growth. *Journal of Extracellular Vesicles*, *4*, 26373–26373. https://doi.org/10.3402/jev.v4.26373

Ezzat, K., Pernemalm, M., Pålsson, S., Roberts, T. C., Järver, P., Dondalska, A., Bestas, B., Sobkowiak, M. J., Levänen, B., Sköld, M., Thompson, E. A., Saher, O., Kari, O. K., Lajunen, T., Sverremark Ekström, E., Nilsson, C., Ishchenko, Y., Malm, T., Wood, M. J. A.…El Andaloussi, S. (2019). The viral protein corona directs viral pathogenesis and amyloid aggregation. *Nature Communications*, *10*(1), 2331. https://doi.org/10.1038/s41467-019-10192-2

Giulimondi, F., Digiacomo, L., Pozzi, D., Palchetti, S., Vulpis, E., Capriotti, A. L., Chiozzi, R. Z., Laganà, A., Amenitsch, H., Masuelli, L., Peruzzi, G., Mahmoudi, M., Screpanti, I., Zingoni, A., Caracciolo, G. (2019). Interplay of protein corona and immune cells controls blood residency of liposomes. *Nature Communications*. *10*(1), 3686–3686. https://doi.org/10.1038/s41467-019-11642-7

Gunnarsson, S. B., Bernfur, K., Mikkelsen, A., & Cedervall, T. (2018). Analysis of nanoparticle biomolecule complexes. *Nanoscale*, *10*(9), 4246–4257. https://doi.org/10.1039/c7nr08696b

György, B., Módos, K., & Pállinger, E. *et al*. (2011). Detection and isolation of cell-derived microparticles are compromised by protein complexes resulting from shared biophysical parameters. *Blood*, *117*(4), e39–48. https://doi.org/10.1182/blood-2010-09-307595

György, B., Pálóczi, K., Kovács, A., Barabás, E., Bekő, G., Várnai, K., Pállinger, É., Szabó-Taylor, K., Szabó, T. G., Kiss, A. A., Falus, A., & Buzás, E. I. (2014). Improved circulating microparticle analysis in acid-citrate dextrose (ACD) anticoagulant tube. *Thrombosis Research*, *133*(2), 285–292. https://doi.org/10.1016/j.thromres.2013.11.010

György, B., Szabó, T. G., Pásztói, M., Pál, Z., Misják, P., Aradi, B., László, V., Pállinger, É., Pap, E., Kittel, Á., Nagy, G., Falus, A., & Buzás, E. I. (2011).Membrane vesicles, current state-of-the-art: Emerging role of extracellular vesicles. *Cellular and Molecular Life Sciences*.;*68*(16), 2667–2688. https://doi.org/10.1007/s00018-011-0689-3

György, B., Szabó, T. G., Turiák, L., Wright, M., Herczeg, P., Ledeczi, Z., Kittel, Á., Polgár, A., Tóth, K., Dérfalvi, B., Zelenák, G., Böröcz, I., Carr, B., Nagy, G., Vékey, K., Gay, S., Falus, A., & Buzás, E. I. (2012). Improved flow cytometric assessment reveals distinct microvesicle (cell-derived microparticle) signatures in joint diseases. *Plos One*, *7*(11), e49726. https://doi.org/10.1371/journal.pone.0049726

Heberle, H., Meirelles, G. V., Da Silva, F. R., Telles, G. P., & Minghim, R. (2015). InteractiVenn: A web-based tool for the analysis of sets through Venn diagrams. *BMC Bioinformatics*, *16*(1), 169. https://doi.org/10.1186/s12859-015-0611-3

Hellstrand, E., Lynch, I., Andersson, A., Drakenberg, T., Dahlbäck, B., Dawson, K. A., Linse, S., & Cedervall, T. (2009). Complete high-density lipoproteins in nanoparticle corona. *The Febs Journal*, *276*(12), 3372–3381. https://doi.org/10.1111/j.1742-4658.2009.07062.x

Jang, Su C., Crescitelli, R., Cvjetkovic, A., Belgrano, V., Olofsson Bagge, R., Sundfeldt, K., Ochiya, T., Kalluri, R., & Lötvall, J. (2019). Mitochondrial protein enriched extracellular vesicles discovered in human melanoma tissues can be detected in patient plasma. *Journal of Extracellular Vesicles*, *8*(1), 1635420–1635420. https://doi.org/10.1080/20013078.2019.1635420

Kalra, H., Simpson, R. J., Ji, H., Aikawa, E., Altevogt, P., Askenase, P., Bond, V. C., Borràs, F. E., Breakefield, X., Budnik, V., Buzas, E., Camussi, G., Clayton, A., Cocucci, E., Falcon-Perez, J. M., Gabrielsson, S., Gho, Y. S., Gupta, D., Harsha, H. C.…Mathivanan, S. (2012). Vesiclepedia: A compendium for extracellular vesicles with continuous community annotation. *Plos Biology*, *10*(12), e1001450. https://doi.org/10.1371/journal.pbio.1001450

Kapralov, A A., Feng, W. H., Amoscato, A A., Yanamala, N., Balasubramanian, K., Winnica, D E., Kisin, E R., Kotchey, G P., Gou, P., Sparvero, L J., Ray, P., Mallampalli, R K., Klein-Seetharaman, J., Fadeel, B., Star, A., Shvedova, A A., & Kagan, V E. (2012). Adsorption of surfactant lipids by single-walled carbon nanotubes in mouse lung upon pharyngeal aspiration. *ACS Nano*, *6*(5), 4147–4156. https://doi.org/10.1021/nn300626q

Karimi, N., Cvjetkovic, A., Jang, Su C., Crescitelli, R., Hosseinpour Feizi, M. A., Nieuwland, R., Lötvall, J., & Lässer, C. (2018). Detailed analysis of the plasma extracellular vesicle proteome after separation from lipoproteins. *Cellular and Molecular Life Sciences*, *75*(15), 2873–2886. https://doi.org/10.1007/s00018-018-2773-4

Kim, D. K., Kang, B., Kim, Oh Y., Choi, D. S., Lee, J., Kim, S. R., Go, G., Yoon, Y. J., Kim, Ji H., Jang, Su C., Park, K-Su, Choi, E. J., Kim, K. P., Desiderio, D. M., Kim, Y. K., Lötvall, J., Hwang, D., & Gho, Y. S. (2013). EVpedia: An integrated database of high-throughput data for systemic analyses of extracellular vesicles. *Journal of Extracellular Vesicles*, *2*, 20384. https://doi.org/10.3402/jev.v2i0.20384

Kowal, J., Arras, G., Colombo, M., Jouve, M., Morath, J. P., Primdal-Bengtson, B., Dingli, F., Loew, D., Tkach, M., & Théry, C. (2016). Proteomic comparison defines novel markers to characterize heterogeneous populations of extracellular vesicle subtypes. *PNAS*, *113*(8), E968–E977. https://doi.org/10.1073/pnas.1521230113

La Barbera, G., Capriotti, A. L., Caracciolo, G., Cavaliere, C., Cerrato, A., Montone, C. M., Piovesana, S., Pozzi, D., Quagliarini, E., & Laganà, A. (2020). A comprehensive analysis of liposomal biomolecular corona upon human plasma incubation: The evolution towards the lipid corona. *Talanta*, *209*, 120487. https://doi.org/10.1016/j.talanta.2019.120487

Lacroix, R., Judicone, C., Mooberry, M., Boucekine, M., Key, N. S., & Dignat-George, F. (2013). The ISTH SSC Workshop. Standardization of pre-analytical variables in plasma microparticle determination: Results of the International Society on Thrombosis and Haemostasis SSC Collaborative workshop. *Journal of Thrombosis and Haemostasis*, 1190–1193. https://doi.org/10.1111/jth.12207

Lee, Ju Y., Wang, H., Pyrgiotakis, G., Deloid, G. M., Zhang, Z., Beltran-Huarac, J., Demokritou, P., & Zhong, W. (2018). Analysis of lipid adsorption on nanoparticles by nanoflow liquid chromatography-tandem mass spectrometry. *Analytical and Bioanalytical Chemistry*, *410*(24), 6155–6164. https://doi.org/10.1007/s00216-018-1145-0

Liao, Z., Muth, D. C., Eitan, E., Travers, M., Learman, L. N., Lehrmann, E., & Witwer, K. W. (2017). Serum extracellular vesicle depletion processes affect release and infectivity of HIV-1 in culture. *Scientific Reports*, *7*(1), 2558–2558. https://doi.org/10.1038/s41598-017-02908-5

Lötvall, J., Hill, A. F., Hochberg, F., Buzás, E. I., Di Vizio, D., Gardiner, C., Gho, Y. S., Kurochkin, I. V., Mathivanan, S., Quesenberry, P., Sahoo, S., Tahara, H., Wauben, M. H., Witwer, K. W., & Théry, C. (2014). Minimal experimental requirements for definition of extracellular vesicles and their functions: A position statement from the International Society for Extracellular Vesicles. *Journal Extracellular Vesicles*, 26913. https://doi.org/10.3402/jev.v3.26913

Mahler, H. C., Friess, W., Grauschopf, U., Kiese, S. (2009). Protein aggregation: Pathways, induction factors and analysis. *Journal of Pharmaceutical Sciences*, *98*(9), 2909–2934. https://doi.org/10.1002/jps.21566

Martel, J., Wu, C. Y., Hung, C-Yu, Wong, T. Y., Cheng, A. J., Cheng, M. L., Shiao, M. S., & Young, J. D. (2016). Fatty acids and small organic compounds bind to mineralo-organic nanoparticles derived from human body fluids as revealed by metabolomic analysis. *Nanoscale*, *8*(10), 5537–5545. https://doi.org/10.1039/C5NR08116E

Müller, J., Prozeller, D., Ghazaryan, A., Kokkinopoulou, M., Mailänder, V., Morsbach, S., & Landfester, K. (2018). Beyond the protein corona - lipids matter for biological response of nanocarriers. *Acta Biomaterialia*, *71*, 420–431. https://doi.org/10.1016/j.actbio.2018.02.036

Nakai, W., Yoshida, T., Diez, D., Miyatake, Y., Nishibu, T., Imawaka, N., Naruse, K., Sadamura, Y., & Hanayama, R. (2016). A novel affinity-based method for the isolation of highly purified extracellular vesicles. *Scientific Reports*, *6*(1), 33935. https://doi.org/10.1038/srep33935

Németh, A., Orgovan, N., Sódar, B. W., Osteikoetxea, X., Pálóczi, K., Szabó-Taylor, K. É., Vukman, K. V., Kittel, Á., Turiák, L., Wiener, Z., Tóth, S., Drahos, L., Vékey, K., Horvath, R., & Buzás, E. I. (2017). Antibiotic-induced release of small extracellular vesicles (exosomes) with surface-associated DNA. *Scientific Reports*, *7*(1), 8202. https://doi.org/10.1038/s41598-017-08392-1

Nolte-'t Hoen, E., Cremer, T., & Gallo, R. C. et al. (2016).Extracellular vesicles and viruses: Are they close relatives? *Proceedings of the National Academy of Sciences*, *113*(33), 9155. https://doi.org/10.1073/pnas.1605146113

Onódi, Z., Pelyhe, C., Terézia Nagy, C., Brenner, G. B., Almási, L., Kittel, Á., Manček-Keber, M., Ferdinandy, P., Buzás, E. I., Giricz, Z., & Terézia Nagy, C. (2018). Isolation of high-purity extracellular vesicles by the combination of iodixanol density gradient ultracentrifugation and bind-elute chromatography from blood plasma. *Front Physiology*, *9*, 1479–1479. https://doi.org/10.3389/fphys.2018.01479

Osteikoetxea, X., Balogh, A., Szabó-Taylor, K., Németh, A., Szabó, T. G., Pálóczi, K., Sódar, B., Kittel, Á., György, B., Pállinger, É., Matkó, J., & Buzás, E. I. (2015).Improved characterization of EV preparations based on protein to lipid ratio and lipid properties. *Plos One*, *10*(3), e0121184. https://doi.org/10.1371/journal.pone.0121184

Osteikoetxea, X., Sódar, B., Németh, A., Szabó-Taylor, K., Pálóczi, K., Vukman, K. V., Tamási, V., Balogh, A., Kittel, Á., Pállinger, É., & Buzás, E. I. (2015). Differential detergent sensitivity of extracellular vesicle subpopulations. *Organic & Biomolecular Chemistry*, *13*(38), 9775–9782. https://doi.org/10.1039/c5ob01451d

Palviainen, M., Saraswat, M., Varga, Z., Kitka, D., Neuvonen, M., Puhka, M., Joenväärä, S., Renkonen, R., Nieuwland, R., Takatalo, M., & Siljander, P. R. M. (2020). Extracellular vesicles from human plasma and serum are carriers of extravesicular cargo-Implications for biomarker discovery. *Plos One*, *15*(8), e0236439. https://doi.org/10.1371/journal.pone.0236439

Papafilippou, L., Claxton, A., Dark, P., Kostarelos, K., & Hadjidemetriou, M. (2020). Protein corona fingerprinting to differentiate sepsis from non-infectious systemic inflammation [10.1039/D0NR02788J]. *Nanoscale*, *12*(18), 10240–10253. https://doi.org/10.1039/D0NR02788J

Papp, K., Végh, P., Prechl, J., Kerekes, K., Kovács, J., Csikós, G., Bajtay, Z., & Erdei, A. (2008). B lymphocytes and macrophages release cell membrane deposited C3-fragments on exosomes with T cell response-enhancing capacity. *Molecular Immunology*, *45*(8), 2343–2351. https://doi.org/10.1016/j.molimm.2007.11.021

Pathan, M., Keerthikumar, S., Ang, C. S., Gangoda, L., Quek, C. Y.J., Williamson, N. A., Mouradov, D., Sieber, O. M., Simpson, R. J., Salim, A., Bacic, A., Hill, A. F., Stroud, D. A., Ryan, M. T., Agbinya, J. I., Mariadason, J. M., Burgess, A. W., & Mathivanan, S. (2015). FunRich: An open access standalone functional enrichment and interaction network analysis tool. *Proteomics*, *15*(15), 2597–2601. https://doi.org/10.1002/pmic.201400515

Pathan, M., Keerthikumar, S., Chisanga, D., Alessandro, R., Ang, C. -. S., Askenase, P., Batagov, A O., Benito-Martin, A., Camussi, G., Clayton, A., Collino, F., Di Vizio, D., Falcon-Perez, J. M., Fonseca, P., Fonseka, P., Fontana, S., Gho, Y. S., Hendrix, An, Nolte-'t Hoen, E.…S. (2017). Mathivanan, A novel community driven software for functional enrichment analysis of extracellular vesicles data. *Journal of Extracellular Vesicles*, *6*(1), 1321455. https://doi.org/10.1080/20013078.2017.1321455

Perez-Riverol, Y., Csordas, A., Bai, J., Bernal-Llinares, M., Hewapathirana, S., Kundu, D. J., Inuganti, A., Griss, J., Mayer, G., Eisenacher, M., Pérez, E., Uszkoreit, J., Pfeuffer, J., Sachsenberg, T., Yılmaz, Ş., Tiwary, S., Cox, J., Audain, E., Walzer, M.…Vizcaíno, J. A. (2019). The PRIDE database and related tools and resources in 2019: Improving support for quantification data. *Nucleic Acids Research*, *47*(D1), D442–D450. https://doi.org/10.1093/nar/gky1106

Pink, M., Verma, N., Kersch, C., & Schmitz-Spanke, S. (2018). Identification and characterization of small organic compounds within the corona formed around engineered nanoparticles. *Environmental Science: Nano*, *5*(6), 1420–1427. https://doi.org/10.1039/C8EN00161H

Raesch, S. S., Tenzer, S., Storck, W., Rurainski, A., Selzer, D., Ruge, C. A., Perez-Gil, J., Schaefer, U. F., & Lehr, C. M. (2015).Proteomic and lipidomic analysis of nanoparticle corona upon contact with lung surfactant reveals differences in protein, but not lipid composition. *ACS Nano*, *9*(12), 11872–11885. https://doi.org/10.1021/acsnano.5b04215

Shelke, G. V., Lässer, C., Gho, Y. S., & Lötvall, J. (2014). Importance of exosome depletion protocols to eliminate functional and RNA-containing extracellular vesicles from fetal bovine serum. *Journal of Extracellular Vesicles*, *3*, 24783. https://doi.org/10.3402/jev.v3.24783

Skliar, M., Chernyshev, V. S., Belnap, D. M., Sergey, G. V., Al-Hakami, S. M., Bernard, P. S., Stijleman, I. J., & Rachamadugu, R. (2018). Membrane proteins significantly restrict exosome mobility. *Biophysical Research Communications*, *501*(4), 1055–1059. https://doi.org/10.1016/j.bbrc.2018.05.107

Sódar, B. W., Kittel, Á., Pálóczi, K., Vukman, K. V., Osteikoetxea, X., Szabó-Taylor, K., Németh, A., Sperlágh, B., Baranyai, T., Giricz, Z., Wiener, Z., Turiák, L., Drahos, L., Pállinger, É., Vékey, K., Ferdinandy, P., Falus, A., Buzás, E. I. (2016). Low-density lipoprotein mimics blood plasma-derived exosomes and microvesicles during isolation and detection. *Scientific Reports*, *6*(1), 24316. https://doi.org/10.1038/srep24316

Sugár, S., Turiák, L., Vékey, K., & Drahos, L. (2020). Widespread presence of bovine proteins in human cell lines. *Journal of Mass Spectrometry*, *55*(7), e4464. https://doi.org/10.1002/jms.4464

Sung, B. H., Ketova, T., Hoshino, D., Zijlstra, A., & Weaver, A. M. (2015). Directional cell movement through tissues is controlled by exosome secretion. *Nature Communications*, *6*(1), 7164. https://doi.org/10.1038/ncomms8164

Szabó, G. T., Tarr, B., Pálóczi, K., Éder, K., Lajkó, E., Kittel, Á., Tóth, S., György, B., Pásztói, M., Németh, A., Osteikoetxea, X., Pállinger, É., Falus, A., Szabó-Taylor, K., & Buzás, E. I. (2014). Critical role of extracellular vesicles in modulating the cellular effects of cytokines. *Cellular and Molecular Life Sciences*, *71*(20), 4055–4067. https://doi.org/10.1007/s00018-014-1618-z

Szabó-Taylor, K. É., Tóth, E. Á., Balogh, A. M., Sódar, B. W., Kádár, L., Pálóczi, K., Fekete, N., Németh, A., Osteikoetxea, X., Vukman, K. V., Holub, M., Pállinger, É., Nagy, G. Y., Winyard, P. G., & Buzás, E. I. (2017). Monocyte activation drives preservation of membrane thiols by promoting release of oxidised membrane moieties via extracellular vesicles. *Free Radical Biology and Medicine*, *108*, 56–65. https://doi.org/10.1016/j.freeradbiomed.2017.03.016

Szklarczyk, D., Gable, A. L., Lyon, D., Junge, A., Wyder, S., Huerta-Cepas, J., Simonovic, M., Doncheva, N. T., Morris, J. H., Bork, P., Jensen, L. J., & Mering, C. V. (2019). STRING v11: Protein-protein association networks with increased coverage, supporting functional discovery in genome-wide experimental datasets. *Nucleic Acids Research*, *47*(D1), D607–D613. https://doi.org/10.1093/nar/gky1131

Théry, C., Witwer, K. W., Aikawa, E., Alcaraz, M. J., Anderson, J. D., Andriantsitohaina, R., Antoniou, A., Arab, T., Archer, F., Atkin-Smith, G. K., Ayre, D. C., Bach, J.-.M., Bachurski, D., Baharvand, H., Balaj, L., Baldacchino, S., Bauer, N. N., Baxter, A. A., Bebawy, M.…Zuba-Surma, E. K. (2018). Minimal information for studies of extracellular vesicles 2018 (MISEV2018): A position statement of the International Society for Extracellular Vesicles and update of the MISEV2014 guidelines. *Journal of Extracellular Vesicles*, *7*(1), 1535750. https://doi.org/10.1080/20013078.2018.1535750

Turiák, L., Misják, P., Szabó, T. G., Aradi, B., Pálóczi, K., Ozohanics, O., Drahos, L., Kittel, Á., Falus, A., Buzás, E. I., & Vékey, K. (2011). Proteomic characterization of thymocyte-derived microvesicles and apoptotic bodies in BALB/c mice. *Journal of Proteomics*, *74*(10), 2025–2033. https://doi.org/10.1016/j.jprot.2011.05.023

Valadi, H., Ekström, K., Bossios, A., Sjöstrand, M., Lee, J. J., & Lötvall, J. O. (2007). Exosome-mediated transfer of mRNAs and microRNAs is a novel mechanism of genetic exchange between cells. *Nature Cell Biology*, *9*(6), 654–659. https://doi.org/10.1038/ncb1596

van der Pol, E., Sturk, A., & van Leeuwen, T., Nieuwland, R., Coumans, F., & ISTH-SSC-VB Working group. (2018). Standardization of extracellular vesicle measurements by flow cytometry through vesicle diameter approximation. *Journal of Thrombosis and Haemostasis*, *16*(6), 1236–1245. https://doi.org/10.1111/jth.14009

Van Deun, J., Mestdagh, P., Agostinis, P., Akay, Ö., Anand, S., Anckaert, J., Martinez, Z. A., Baetens, T., Beghein, E., Bertier, L., Berx, G., Boere, J., Boukouris, S., Bremer, M., Buschmann, D., Byrd, J. B., Casert, C., Cheng, L., Cmoch, A.…Hendrix, An (2017). EV-TRACK: Transparent reporting and centralizing knowledge in extracellular vesicle research. *Nature Methods*, *14*(3), 228–232. https://doi.org/10.1038/nmeth.4185

Van Deun, J., Mestdagh, P., Sormunen, R., Cocquyt, V., Vermaelen, K., Vandesompele, Jo, Bracke, M., De Wever, O., & Hendrix, An (2014). The impact of disparate isolation methods for extracellular vesicles on downstream RNA profiling. *Journal of Extracellular Vesicles*, *3*, 24858. https://doi.org/10.3402/jev.v3.24858

Varga, Z., Fehér, B., Kitka, D., Wacha, A., Bóta, A., Berényi, S., Pipich, V., & Fraikin, J. L. (2020). Size measurement of extracellular vesicles and synthetic liposomes: The impact of the hydration shell and the protein corona. *Colloids and Surfaces. B, Biointerfaces*, *192*, 111053. https://doi.org/10.1016/j.colsurfb.2020.111053

Vella, L. J., Scicluna, B. J., Cheng, L., Bawden, E. G., Masters, C. L., Ang, C. S., Willamson, N., Mclean, C., Barnham, K. J., & Hill, A. F. (2017). A rigorous method to enrich for exosomes from brain tissue. *Journal of Extracellular Vesicles*, *6*(1), 1348885–1348885. https://doi.org/10.1080/20013078.2017.1348885

Visnovitz, T., Osteikoetxea, X., Sódar, B W., Mihály, J., Lőrincz, P., Vukman, K V., Tóth, E. Á., Koncz, A., Székács, I., Horváth, R., Varga, Z., Buzás, E I. (2019). An improved 96 well plate format lipid quantification assay for standardisation of experiments with extracellular vesicles. *Journal of Extracellular Vesicles*, *8*(1), 1565263. https://doi.org/10.1080/20013078.2019.1565263

Weber, C., Simon, J., & Mailänder, V., Morsbach, S., & Landfester, K., (2018). Preservation of the soft protein corona in distinct flow allows identification of weakly bound proteins. *Acta Biomaterialia*, *76*, 217–224. https://doi.org/10.1016/j.actbio.2018.05.057

Willis, C. M., Nicaise, A. M., Menoret, A., Ryu, J. K., Mendiola, A. S., Jellison, E. R., Givogri, M. I., Han, D. K., Bongarzone, E. R., Akassoglou, K., Vella, A. T., & Crocker, S. J. (2019). Extracellular vesicle fibrinogen induces encephalitogenic CD8+ T cells in a mouse model of multiple sclerosis. *Pnas*, *116*(21), 10488. https://doi.org/10.1073/pnas.1816911116

Xiao, W., Gao, H.. (2018). The impact of protein corona on the behavior and targeting capability of nanoparticle-based delivery system. *International Journal of Pharmaceutics*, *552*(1-2), 328–339. https://doi.org/10.1016/j.ijpharm.2018.10.011

SUPPORTING INFORMATION

Additional supporting information may be found in the online version of the article at the publisher's website.

How to cite this article: Tóth, E. Á., Turiák, L.,Visnovitz, T., Cserép, C., Mázló, A., Sódar, B. W., Försönits, A. I., Petővári, G., Sebestyén, A., Komlósi, Z., Drahos, L., Kittel, Á., Nagy, G., Bácsi, A., Dénes, Á.,Gho, Y. S., Szabó-Taylor, K. É., & Buzás, E. I. (2021). Formation of a protein corona on the surface of extracellular vesicles in blood plasma. *Journal of Extracellular Vesicles*, *10,* e12140. https://doi.org/10.1002/jev2.12140